and A21–178 in Chiba University. Doxorubicin (10 mg/kg body weight) was intraperitoneally injected into wild-type male mice (C57BL/6) once-weekly at weeks 7 and 8 after birth. After both Doxorubicin injections, the mice were reared for a further 2 weeks, and the surviving mice were used for experiments. Myocardial infarction models were prepared using wild-type male mice (C57BL/6) as previously described [11]. Serum and Gr-1(+) cells were isolated 4 weeks after inducing myocardial infarction (11 weeks of age).

Generation of EGFRdn mice. The C-terminal 533 amino acids [42] were deleted from the full-length human *EGFR* cDNA (a gift from Professor T. Kadowaki, The University of Tokyo) by introducing a stop codon (TGA) after the R677 codon by site-directed mutagenesis. The truncated *EGFR* (*EGFRdn*) cDNA was then subcloned into the *αMHC* promoter-containing expression vector (a gift from Professor J. Robbins, Cincinnati Children's Hospital). The 8.2-kb DNA fragment was microinjected as a transgene into pronuclei of eggs from BDF1 mice. The eggs were then transferred into the oviducts of pseudopregnant ICR mice. The transgenic founders were identified by Southern blot and PCR analysis. Line 2–5 and Line 9–12 were established and maintained by breeding to C57BL/6 mice. Line 9–12 was selected for further analysis on the basis of a higher level of transgene expression.

BMMNC infusion and CM injection. BMMNC (2.0×10^7) isolated from a male wild-type mouse and suspended in 200 μl of PBS or an equal volume of PBS as a control were injected into the tail veins of anesthetized (4% inhaled isoflurane) 8-week-old male EGFRdn mice and 11-week-old male DOX and OMI mice. CM (200 μl) from Gr-1(+) cells from male wild-type mice or isovolume serum-depleted DMEM were infused into the tail veins of anesthetized 8-week-old male EGFRdn mice and 11-week-old male DOX mice under anesthesia. Anti-mouse insulin-like growth factor-1 (IGF-1) (0.1 μg/g body weight) or anti-goat immunoglobulin G (IgG) (0.1 μg/g body weight) antibodies were intraperitoneally injected into 11-week-old male DOX mice 2 h before CM infusion. Anti-activin A (20 μg) or anti-mouse IgG (20 μg) antibodies were intraperitoneally injected at 48-h intervals into male EGFRdn mice from 10 to 12 weeks of age. Pegvisomant (10 mg/kg body weight) or vehicle (control) were intraperitoneally injected into 8-week-old male DOX mice 30 min before CM infusion.

Evaluation of cell shortening and the beating rate of cardiomyocytes. After 12 h starvation with 500 μl serum-depleted DMEM in 12-well dishes, rat cardiomyocytes were cultured with 500 μl of CM or serum-depleted DMEM. At specific times, the cultured cardiomyocytes were video recorded for 10 sec, and the percentage of cell shortening was analyzed using ImageExpress version 5.5 (Nippon Roper). To measure the percentage of cell shortening, two regions of interest were fixed by the software, which analyzed the beating distance of a single cardiomyocyte, and divided the distance by the length between the regions of interest. The number of beats of single cardiomyocyte was counted for 10 sec to determine the beating rate. For antibody treatment *in vitro*, the starved cardiomyocytes were pretreated with anti-IGF-1 (10 μg/ml) or anti-goat IgG (10 μg/ml) antibodies for 2 h before adding CM. For pegvisomant treatment *in vitro*, the cardiomyocytes were pretreated with pegvisomant (12.5 μg/ml) for 30 min before adding CM.

Echocardiography and catheterization. Transthoracic echocardiographic analysis and catheterization analysis were performed as previously described [11]_ENREF_9. Briefly, the +dp/dt in the left ventricle was measured using a catheter, which was introduced retrogradely *via* the carotid artery.

Cell isolation. Neonatal rat cardiomyocytes were isolated and separately collected as described previously [43]. Cardiomyocytes were plated at a density of 1×10^5 cells/cm^2 on six-, 12- and 24-well dishes (BD Falcon) coated with 1% gelatin and cultured in DMEM supplemented with 10% FBS. Adult cardiomyocytes were prepared as previously described [44]. BMMNC and PBMNC were isolated from 8-week-old male C57BL/6, male GFP mice, and male EGFRdn mice by density gradient centrifugation with Histopaque-1083, as previously described [45]. PBMNC were also isolated from human subjects, as previously described [46].

Sorting of harvested BMMNC into sub-populations and collection of CM. After BMMNC were harvested from male wild-type mice, the cells were sorted into Gr-1(+) cells, B220(+) cells, TER(+) cells, and lineage-negative populations using a Magnetic Cell Sorting system (Miltenyi Biotec), as previously described [47]. To collect the CM, the individual sub-populations were seeded onto 24-well dishes with 200 μl of serum-depleted DMEM. After incubation for 24 h in serum-depleted DMEM, the supernatant (CM) was collected, and any cells were removed by filtering through a 0.45-μm filter (BD Falcon).

Phase-contrast live imaging. Live images of beating cardiomyocytes were taken using a Leica inverted microscope (Leica) equipped with a phase-contrast objective and a CCD camera (Leica).

Flow cytometry. The percentage of cells expressing each cell surface antigen was analyzed using a FACSCalibur (Becton Dickinson Immunocytometry Systems) and Cell Quest Pro version 5.2 software.

RNA extraction and DNA microarray analysis. Total RNA was extracted from 12-week-old male wild-type ($n=4$) and age-matched male EGFRdn mice ($n=4$) using a RNeasy Mini Kit (Qiagen) according to the manufacturer's protocol. RNA quality was assessed with an Agilent 2100 Bioanalyzer (Agilent Technologies). cRNA preparation, fragmentation, hybridization, and scanning of a GeneChip® Mouse Genome 430 2.0 Arrays (Affymetrix) were performed according to the manufacturer's protocol. cRNA was labeled using a Two-cycle Eukaryotic Target Labeling assay with a GeneChip Expression 3′ amplification two-cycle labeling and control reagents kit (Affymetrix). Briefly, cDNA was generated from total RNA (100 ng) using SuperScript II (Invitrogen) and a T7-oligo(dT) promoter primer (Affymetrix). After second-strand cDNA synthesis, cDNA was converted to cRNA by an *in vitro* transcription reaction (MEGAscript T7 kit, Ambion). The cRNA was then purified using a Sample Cleanup Module (Affymetrix), and the yield was monitored with a spectrophotometer. The second cycle of cDNA synthesis was performed, followed by the same cleanup as above and a second *in vitro* transcription reaction cycle with biotin-labeled ribonucleotides and T7 RNA polymerase. The labeled cRNA was purified, using a Sample Cleanup Module and denatured at 94°C before hybridization. The samples were hybridized to GeneChip® Mouse Genome 430 2.0 Arrays at 45°C for 16 h with rotation at 60 rpm. The arrays were then washed, stained with phycoerythrin–streptavidin (Molecular Probes), washed, and scanned with a GeneChip Scanner 3000 7G (Affymetrix). The data were analyzed with GeneSpring version 7.3.1 software (Agilent Technologies).

Reverse transcriptase-PCR. RNA extraction and RT-PCR were performed as previously described [11]. Real-time PCR amplification was performed using an Applied Biosystems 7500 real-time PCR system (Applied Biosystems) with QuantiTect SYBR Green PCR Master Mix (Qiagen). The PCR protocol comprised an initial denaturation step (94°C, 15 sec) followed by 60 cycles of amplification and quantification (55°C for 30 sec and 72°C for 35 sec) and a melting curve program (60–95°C). The

relative mRNA expression level was calculated using the standard curve of GAPDH. All samples were independently analyzed at least three times for each gene. Semi-quantitative RT-PCR of GH was performed using 0.4 μg of total RNA and followed by 40 cycles of the above conditions. The primer sequences were QT00311654 (Qiagen) for GH in real-time PCR, 5′-TCCTG-TGGACAGATCACTGC-3′ and 5′-AATGTAGGCACGCTC-GAACT-3′ for GH in semi-quantitative PCR, QT00309099 (Qiagen) for GAPDH, and 5′-GGACCTGGCTGGCCGGGA-CC-3′ and 5′-GCGGTGCACGATGGAGGGGC-3′ for β-actin. For semi-quantitative RT-PCR, the PCR products were size-fractionated by 2% agarose gel electrophoresis.

Northern blot analysis. For northern blot analysis, total RNA (20 μg) was extracted from hearts using TRIzol Reagent (Invitrogen) and hybridized with a cDNA probe for *EGFRdn*. 18S rRNA ethidium bromide staining was used to quantify RNA loading.

Analysis of phosphorylated ErbB receptor expression. Four-week-old mice were anesthetized by intraperitoneal injection of urethane (2 mg/g body weight) followed by intravenous injection of HB-EGF (0.5 μg/g body weight, R&D Systems), NRG-1β (0.5 μg/g body weight, R&D Systems), or vehicle *via* the inferior vena cava. After 5 min, the hearts were immediately excised and homogenized in a buffer containing 50 mmol/l HEPES (pH 7.5), 137 mmol/l NaCl, 1 mmol/l $MgCl_2$, 1 mmol/l $CaCl_2$, 10 mmol/l Na-pyrophosphate, 2 mmol/l EDTA, 1% NP-40, 10% glycerol, 2 mmol/l Na_3VO_4, 10 mmol/l NaF, and protease inhibitor cocktail (Complete Mini, Roche Applied Science). To analyze the tyrosine phosphorylation of ErbB receptors, equivalent amounts of proteins were subjected to immunoprecipitation with the specific antibodies, fractionated by 6% SDS-PAGE, and immunoblotted with the mouse monoclonal anti-phosphotyrosine antibody 4G10 (Millipore). Horseradish peroxidase-conjugated anti-mouse IgG antibody (GE Healthcare) was used as the secondary antibody, and the bound antibodies were detected using an ECL detection kit (GE Healthcare).

ELISA. Serum and CM concentrations of cAMP, GH and activin A were measured by ELISA (cAMP and activin A, R&D Systems; GH, LINCO Research). To prepare cell lysates for cAMP analysis, cardiomyocytes were seeded (4×10^5 cells/cm) onto six-well dishes coated with 1% gelatin and cultured in DMEM supplemented with 10% FBS. After 5 d, the cells were washed three times with PBS and the medium was changed to serum-depleted DMEM. After incubation for 12 h in the serum-depleted medium, the cells were washed three times with PBS and the medium was replaced with 1 ml of serum-depleted DMEM with CM (1 ml), 2 ml of serum-depleted DMEM with 500 pg/ml GH, 2 ml of serum-depleted DMEM with 12.5 μg/ml pegvisomant, or 1 ml of serum-depleted DMEM plus 1 ml of CM and 12.5 μg/ml pegvisomant. Thirty minutes later, the cardiomyocytes were resuspended in lysis buffer in six-well dish.

To examine the expression of NFκB and phosphorylated NFκB in PBMNC, PBMNC isolated from wild-type male mice were cultured with AngII or TNFα. Thirty minutes later, PBMNC were resuspended in lysis buffer and the expression of NFκB and phosphorylated NFκB were examined using sandwich ELISA kits (Cell Signaling). Some cells were also treated with 50 μM NFκB p65 (Ser276) inhibitory peptide to inhibit NFκB activity.

Western blot analysis. Whole-cell lysates (30–50 μg) were resolved by SDS-PAGE. The separated proteins were transferred to a PVDF membrane (GE Healthcare) and incubated with the primary antibody, followed by an anti-IgG-horseradish peroxidase-conjugated secondary antibody. Proteins were detected using an ECL-Plus kit (GE Healthcare).

Immunohistology. The hearts were fixed with 4% paraformaldehyde and embedded in paraffin, or fixed in 10% neutralized formalin and embedded in Tissue-Tek OCT cryo-embedding compound (Sakura Finetek). The specimens were sectioned (5 μm thick), and stained with hematoxylin/eosin or Masson trichrome.

Evaluation of cardiac hypertrophy. To evaluate the mean diameter of LV cardiomyocytes, the shortest diameter of each cardiomyocyte was measured in nucleated transverse sections stained with hematoxylin-eosin. Thirty cardiomyocytes in each LV were measured using an ocular micrometer disc with a linear scale at a magnification of 400×, and the average cardiomyocyte diameter was calculated for each specimen. Four hearts were measured in each group. The cell surface area of isolated neonatal and adult cardiomyocytes was measured by planimetry in 50 randomly selected cells per specimen.

Immunofluorescence staining. Immunostaining was performed as previously described [45]. Images were taken using a fluorescent microscopy (Leica) with LAS AF software (Leica).

Human subjects. We enrolled 10 subjects who were outpatients of Department of Cardiology of Tokyo Women's Medical University Hospital. We obtained 10 ml of whole blood from each patient. Half of the blood sample was used to measure the serum activin A concentration and the remaining blood was used to measure GH in CM after PBMNC isolation. All patients were receiving medical therapies and exhibited New York Heart Association class II symptoms. We also enrolled 11 healthy age- and body mass index-matched volunteers. Characteristics of the patients and healthy subjects are summarized in Table S1.

Statistics. Data are presented as means ± s.e.m. We examined differences between groups by Student's *t* test or analysis of variance followed by Bonferroni's correction to compare means. A value of $P<0.05$ was considered to be significant.

Supporting Information

Figure S1 Overexpression of EGFRdn inhibited the functional activation of endogenous ErbB receptors in a dominant-negative manner. (A) Northern blot analysis for the transgene expression in hearts from wild-type and two different founder lines of EGFRdn mice (L2–5 and L9–12). (B) Tyrosine phosphorylation of ErbB receptors in hearts from wild-type and EGFRdn mice (L9–12) at 5 min after injection of HB-EGF. In wild-type mice, intravenous injection of HB-EGF enhanced cardiac tyrosine phosphorylation of EGFR, ErbB2 and ErbB4, which was abrogated in EGFRdn hearts. HB-EGF, heparin-binding EGF-like growth factor. (C) Tyrosine phosphorylation of ErbB receptors in hearts from wild-type and EGFRdn mice (L9–12) at 5 min after the injection of NRG-1β. NRG-1β induced tyrosine phosphorylation of ErbB2 and ErbB4 in wild-type hearts, but not in EGFRdn hearts. NRG-1, neuregulin-1.
(TIF)

Figure S2 Echocardiographic analysis of DOX mice. (A) Representative M-mode images of wild-type and DOX mice. (B) Left ventricular diastolic and systolic dimensions, and FS of 11-week-old DOX mice ($n=36$) and age-matched wild-type mice ($n=10$). LVDd, left ventricular diastolic dimension; LVDs, left ventricular systolic dimension. Data are means ± s.e.m.
(TIF)

Figure S3 Analysis of cardiac hypertrophy. (A) The shortest diameter of each cardiomyocyte ($n=30$ per group). Lower photographs, H&E-stained tissue sections. Scale bar, 75 μm. (B) Surface area of isolated adult cardiomyocytes ($n=50$ per group).

Lower photographs, representative images. Scale bar, 75 μm. Data are means ± s.e.m.
(TIF)

Figure S4 Flow cytometric analysis. The left and right panels show the expression of each cell surface marker before and after magnetic sorting (MACS), respectively.
(TIF)

Figure S5 Cardiac hypertrophy *in vitro*. Upper graph, cell surface area of neonatal rat cardiomyocytes ($n = 50$); lower photographs, representative images of the cells. Cardiomyocytes were stained with sarcomeric α-actinin (red). Nuclei were stained with Hoechst 33258 (blue). Scale bars, 75 μm. Data are means ± s.e.m.
(TIF)

Figure S6 Comparison of GH concentration. GH concentration in CM from Gr-1(+) cells isolated from old myocardial infarction (OMI) mice and DOX mice ($n = 5$). Data are means ± s.e.m.
(TIF)

Figure S7 BMMNC improve the cardiac function of OMI mice via the GH receptor. (A) At 4 weeks after coronary ligation, BMMNC were infused via the tail vein. Pegvisomant (10 mg/kg body weight) or vehicle (control) was intraperitoneally injected into OMI mice 30 min before infusing BMMNC. BMMNC infusion improved FS and +dp/dt at 3 d after infusion and these improvements were inhibited by pegvisomant (n = 5). (B) Masson trichrome staining. Panels show representative images. Scale bars: 1 mm. Data are means ± s.e.m.
(TIF)

Figure S8 Direct effects of GH in the CM from Gr-1(+) cells on cardiomyocytes. CM from Gr-1(+) cells from wild-type mice was infused into DOX-treated wild-type mice (wild-DOX) or DOX-treated cardiac-specific STAT3dn mice (STAT3dn-DOX). Gr-1(+) cell-derived CM improved FS (left) and +dp/dt (right) in wild-DOX mice ($n = 5$) at 1 d after infusion, but not in STAT3dn-DOX ($n = 5$). Data are means ± s.e.m.
(TIF)

Figure S9 Serum activin A concentrations ($n = 5$). Data are means ± s.e.m.
(TIF)

Figure S10 TNFα increases the secretion of activin A from PBMNC *via* NFκB. (A) Activin A levels in CM from PBMNC were upregulated by treatment with TNFα ($n = 5$). (B) TNFα (50 ng/ml) activated NFκB in PBMNC ($n = 5$). Left, total NFκB; right, phosphorylated NFκB. (C) TNFα (50 ng/ml) -mediated upregulation of activin A in PBMNC was inhibited by treatment with the NFκB inhibitory peptide ($n = 5$). Isotype peptide was used as control. Data are means ± s.e.m.
(TIF)

Table S1 Characteristics of human subjects.
(PDF)

Acknowledgments

We thank M. Okabe (Osaka University, Japan) for the GFP transgenic mice, K. Yamauchi-Takihara (Osaka University) for the cardiac-specific STAT3dn mice, N. Ueno (Tokyo Women's Medical University) for manuscript preparation, T. Kadowaki (The University of Tokyo, Tokyo), J. Robbins (Children's Hospital, Cincinnati, OH) for providing cDNAs, A. Suzuki and K. Nomura (Tokyo Women's Medical University) for their technical supports, and H. Nagao and K. Yoshihara for their excellent technical assistance.

Author Contributions

Conceived and designed the experiments: KM IK. Performed the experiments: NF KM HA AH TN TT AS KMM. Analyzed the data: NF KM HA. Contributed reagents/materials/analysis tools: TS TO. Wrote the paper: NF KM NH IK.

References

1. Passier R, van Laake LW, Mummery CL (2008) Stem-cell-based therapy and lessons from the heart. Nature 453: 322–329.
2. Schachinger V, Erbs S, Elsasser A, Haberbosch W, Hambrecht R, et al. (2006) Intracoronary bone marrow-derived progenitor cells in acute myocardial infarction. N Engl J Med 355: 1210–1221.
3. Segers VF, Lee RT (2008) Stem-cell therapy for cardiac disease. Nature 451: 937–942.
4. van Ramshorst J, Bax JJ, Beeres SL, Dibbets-Schneider P, Roes SD, et al. (2009) Intramyocardial bone marrow cell injection for chronic myocardial ischemia: a randomized controlled trial. JAMA 301: 1997–2004.
5. Martin-Rendon E, Brunskill SJ, Hyde CJ, Stanworth SJ, Mathur A, et al. (2008) Autologous bone marrow stem cells to treat acute myocardial infarction: a systematic review. Eur Heart J 29: 1807–1818.
6. Donndorf P, Kundt G, Kaminski A, Yerebakan C, Liebold A, et al. (2011) Intramyocardial bone marrow stem cell transplantation during coronary artery bypass surgery: A meta-analysis. J Thorac Cardiovasc Surg.
7. Orlic D, Kajstura J, Chimenti S, Jakoniuk I, Anderson SM, et al. (2001) Bone marrow cells regenerate infarcted myocardium. Nature 410: 701–705.
8. Murry CE, Soonpaa MH, Reinecke H, Nakajima H, Nakajima HO, et al. (2004) Haematopoietic stem cells do not transdifferentiate into cardiac myocytes in myocardial infarcts. Nature 428: 664–668.
9. Cho HJ, Lee N, Lee JY, Choi YJ, Ii M, et al. (2007) Role of host tissues for sustained humoral effects after endothelial progenitor cell transplantation into the ischemic heart. J Exp Med 204: 3257–3269.
10. Gnecchi M, He H, Liang OD, Melo LG, Morello F, et al. (2005) Paracrine action accounts for marked protection of ischemic heart by Akt-modified mesenchymal stem cells. Nat Med 11: 367–368.
11. Matsuura K, Honda A, Nagai T, Fukushima N, Iwanaga K, et al. (2009) Transplantation of cardiac progenitor cells ameliorates cardiac dysfunction after myocardial infarction in mice. J Clin Invest 119: 2204–2217.
12. Muller AF, Kopchick JJ, Flyvbjerg A, van der Lely AJ (2004) Clinical review 166: Growth hormone receptor antagonists. J Clin Endocrinol Metab 89: 1503–1511.
13. Funamoto M, Fujio Y, Kunisada K, Negoro S, Tone E, et al. (2000) Signal transducer and activator of transcription 3 is required for glycoprotein 130-mediated induction of vascular endothelial growth factor in cardiac myocytes. J Biol Chem 275: 10561–10566.
14. Bodner M, Castrillo JL, Theill LE, Deerinck T, Ellisman M, et al. (1988) The pituitary-specific transcription factor GHF-1 is a homeobox-containing protein. Cell 55: 505–518.
15. Ingraham HA, Chen RP, Mangalam HJ, Elsholtz HP, Flynn SE, et al. (1988) A tissue-specific transcription factor containing a homeodomain specifies a pituitary phenotype. Cell 55: 519–529.
16. Gaddy-Kurten D, Vale WW (1995) Activin increases phosphorylation and decreases stability of the transcription factor Pit-1 in MtTW15 somatotrope cells. J Biol Chem 270: 28733–28739.
17. Yndestad A, Ueland T, Oie E, Florholmen G, Halvorsen B, et al. (2004) Elevated levels of activin A in heart failure: potential role in myocardial remodeling. Circulation 109: 1379–1385.
18. Schrier RW, Abraham WT (1999) Hormones and hemodynamics in heart failure. N Engl J Med 341: 577–585.
19. Takahashi M, Suzuki E, Takeda R, Oba S, Nishimatsu H, et al. (2008) Angiotensin II and tumor necrosis factor-alpha synergistically promote monocyte chemoattractant protein-1 expression: roles of NF-kappaB, p38, and reactive oxygen species. Am J Physiol Heart Circ Physiol 294: H2879–2888.
20. Gao LR, Wang ZG, Zhu ZM, Fei YX, He S, et al. (2006) Effect of intracoronary transplantation of autologous bone marrow-derived mononuclear cells on outcomes of patients with refractory chronic heart failure secondary to ischemic cardiomyopathy. Am J Cardiol 98: 597–602.
21. Bartke A (2005) Minireview: role of the growth hormone/insulin-like growth factor system in mammalian aging. Endocrinology 146: 3718–3723.
22. Giustina A, Lorusso R, Borghetti V, Bugari G, Misitano V, et al. (1996) Impaired spontaneous growth hormone secretion in severe dialated cardiomyopathy. Am Heart J 131: 620–622.
23. Colligan PB, Brown-Borg HM, Duan J, Ren BH, Ren J (2002) Cardiac contractile function is enhanced in isolated ventricular myocytes from growth hormone transgenic mice. J Endocrinol 173: 257–264.
24. Tajima M, Weinberg EO, Bartunek J, Jin H, Yang R, et al. (1999) Treatment with growth hormone enhances contractile reserve and intracellular calcium

transients in myocytes from rats with postinfarction heart failure. Circulation 99: 127–134.
25. Bueno OF, De Windt LJ, Tymitz KM, Witt SA, Kimball TR, et al. (2000) The MEK1-ERK1/2 signaling pathway promotes compensated cardiac hypertrophy in transgenic mice. EMBO J 19: 6341–6350.
26. Shiojima I, Sato K, Izumiya Y, Schiekofer S, Ito M, et al. (2005) Disruption of coordinated cardiac hypertrophy and angiogenesis contributes to the transition to heart failure. J Clin Invest 115: 2108–2118.
27. Matsui T, Li L, del Monte F, Fukui Y, Franke TF, et al. (1999) Adenoviral gene transfer of activated phosphatidylinositol 3′-kinase and Akt inhibits apoptosis of *hypoxic cardiomyocytes in vitro*. Circulation 100: 2373–2379.
28. Kunisada K, Negoro S, Tone E, Funamoto M, Osugi T, et al. (2000) Signal transducer and activator of transcription 3 in the heart transduces not only a hypertrophic signal but a protective signal against doxorubicin-induced cardiomyopathy. Proc Natl Acad Sci U S A 97: 315–319.
29. Harada M, Qin Y, Takano H, Minamino T, Zou Y, et al. (2005) G-CSF prevents cardiac remodeling after myocardial infarction by activating the Jak-Stat pathway in cardiomyocytes. Nat Med 11: 305–311.
30. Sirotkin AV (2005) Control of reproductive processes by growth hormone: extra- and intracellular mechanisms. Vet J 170: 307–317.
31. Colao A, Vitale G, Pivonello R, Ciccarelli A, Di Somma C, et al. (2004) The heart: an end-organ of GH action. Eur J Endocrinol 151: S93–101.
32. Colao A (2008) The GH-IGF-I axis and the cardiovascular system: clinical implications. Clin Endocrinol 69: 347–358.
33. Welch S, Plank D, Witt S, Glascock B, Schaefer E, et al. (2002) Cardiac-specific IGF-1 expression attenuates dilated cardiomyopathy in tropomodulin-overexpressing transgenic mice. Circ Res 90: 641–648.
34. Torella D, Rota M, Nurzynska D, Musso E, Monsen A, et al. (2004) Cardiac stem cell and myocyte aging, heart failure, and insulin-like growth factor-1 overexpression. Circ Res 94: 514–524.
35. Marleau S, Mulumba M, Lamontagne D, Ong H (2006) Cardiac and peripheral actions of growth hormone and its releasing peptides: relevance for the treatment of cardiomyopathies. Cardiovasc Res 69: 26–35.
36. Le Corvoisier P, Hittinger L, Chanson P, Montagne O, Macquin-Mavier I, et al. (2007) Cardiac effects of growth hormone treatment in chronic heart failure: A meta-analysis. J Clin Endocrinol Metab 92: 180–185.
37. Cicoira M, Kalra PR, Anker SD (2003) Growth hormone resistance in chronic heart failure and its therapeutic implications. J Card Fail 9: 219–226.
38. Anker SD, Chua TP, Ponikowski P, Harrington D, Swan JW, et al. (1997) Hormonal changes and catabolic/anabolic imbalance in chronic heart failure and their importance for cardiac cachexia. Circulation 96: 526–534.
39. Ozcelik C, Erdmann B, Pilz B, Wettschureck N, Britsch S, et al. (2002) Conditional mutation of the ErbB2 (HER2) receptor in cardiomyocytes leads to *dilated cardiomyopathy*. Proc Natl Acad Sci U S A 99: 8880–8885.
40. Seidman A, Hudis C, Pierri MK, Shak S, Paton V, et al. (2002) Cardiac dysfunction in the trastuzumab clinical trials experience. J Clin Oncol 20: 1215–1221.
41. Perez EA, Rodeheffer R (2004) Clinical cardiac tolerability of trastuzumab. J Clin Oncol 22: 322–329.
42. Redemann N, Holzmann B, von Ruden T, Wagner EF, Schlessinger J, et al. (1992) Anti-oncogenic activity of signalling-defective epidermal growth factor receptor mutants. Mol Cell Biol 12: 491–498.
43. Ikeda K, Tojo K, Tokudome G, Hosoya T, Harada M, et al. (2000) The effects of sarpogrelate on cardiomyocyte hypertrophy. Life Sci 67: 2991–2996.
44. Zou Y, Akazawa H, Qin Y, Sano M, Takano H, et al. (2004) Mechanical stress activates angiotensin II type 1 receptor without the involvement of angiotensin II. Nat Cell Biol 6: 499–506.
45. Matsuura K, Wada H, Nagai T, Iijima Y, Minamino T, et al. (2004) Cardiomyocytes fuse with surrounding noncardiomyocytes and reenter the cell cycle. J Cell Biol 167: 351–363.
46. Honda A, Matsuura K, Fukushima N, Tsurumi Y, Kasanuki H, et al. (2009) Telmisartan induces proliferation of human endothelial progenitor cells via PPARgamma-dependent PI3K/Akt pathway. Atherosclerosis 205: 376–384.
47. Matsuura K, Nagai T, Nishigaki N, Oyama T, Nishi J, et al. (2004) Adult cardiac Sca-1-positive cells differentiate into beating cardiomyocytes. J Biol Chem 279: 11384–11391.

Cell Metabolism
Article

p53-Induced Adipose Tissue Inflammation Is Critically Involved in the Development of Insulin Resistance in Heart Failure

Ippei Shimizu,[1,5] Yohko Yoshida,[1,5] Taro Katsuno,[1] Kaoru Tateno,[1] Sho Okada,[1] Junji Moriya,[1] Masataka Yokoyama,[1] Aika Nojima,[1] Takashi Ito,[1] Rudolf Zechner,[2] Issei Komuro,[3] Yoshio Kobayashi,[1] and Tohru Minamino[1,4,*]
[1]Department of Cardiovascular Science and Medicine, Chiba University Graduate School of Medicine, Chiba 260-8670, Japan
[2]Institute of Molecular Biosciences, University of Graz, A-8010 Graz, Austria
[3]Department of Cardiovascular Medicine, Osaka University School of Medicine, Osaka 565-0871, Japan
[4]PRESTO, Japan Science and Technology Agency, Saitama 332-0012, Japan
[5]These authors contributed equally to this work
*Correspondence: t_minamino@yahoo.co.jp
DOI 10.1016/j.cmet.2011.12.006

SUMMARY

Several clinical studies have shown that insulin resistance is prevalent among patients with heart failure, but the underlying mechanisms have not been fully elucidated. Here, we report a mechanism of insulin resistance associated with heart failure that involves upregulation of p53 in adipose tissue. We found that pressure overload markedly upregulated p53 expression in adipose tissue along with an increase of adipose tissue inflammation. Chronic pressure overload accelerated lipolysis in adipose tissue. In the presence of pressure overload, inhibition of lipolysis by sympathetic denervation significantly downregulated adipose p53 expression and inflammation, thereby improving insulin resistance. Likewise, disruption of p53 activation in adipose tissue attenuated inflammation and improved insulin resistance but also ameliorated cardiac dysfunction induced by chronic pressure overload. These results indicate that chronic pressure overload upregulates adipose tissue p53 by promoting lipolysis via the sympathetic nervous system, leading to an inflammatory response of adipose tissue and insulin resistance.

INTRODUCTION

The p53 tumor suppressor pathway coordinates DNA repair, cell-cycle arrest, apoptosis, and senescence to preserve genomic stability and prevent oncogenesis. Activation of p53 is driven by a wide variety of stress signals that have the potential to promote tumor formation, such as DNA damage, telomere shortening, oxidative stress, and oncogene activation (Harris and Levine, 2005; Meek, 2009; Vousden and Prives, 2009). Recently, the contribution of p53 to many undesirable aspects of aging and age-associated diseases, such as cardiovascular and metabolic disorders, has been recognized (Royds and Iacopetta, 2006; Vousden and Lane, 2007). It has been reported that aging is associated with an increase of the p53-mediated transcriptional activity (Edwards et al., 2007) and that slight constitutive overactivation of p53 is associated with premature aging in mice (Maier et al., 2004; Tyner et al., 2002). Activation of p53 has also been observed in aged vessels and failing hearts and has been implicated in atherosclerosis and heart failure (Minamino and Komuro, 2007, 2008; Sano et al., 2007). Recent findings have indicated a role of p53 in determining the response of cells to nutrient stress and in regulating metabolism (Vousden and Ryan, 2009). It has also been demonstrated that excessive calorie intake induces p53-induced inflammation in adipose tissue, leading to insulin resistance and diabetes in mice (Minamino et al., 2009).

A close link between heart failure and diabetes has long been recognized in the clinical setting (Ashrafian et al., 2007; Lopaschuk et al., 2007; Witteles and Fowler, 2008). Many mechanisms have been suggested to explain the increased incidence of heart failure in diabetic patients, including the hypertrophic influence of insulin, the adverse effects of hyperglycemia, increased oxidative stress, and hyperactivity of neurohumoral systems, such as the renin-angiotensin-aldosterone system and the adrenergic system. Recently, increasing attention has been paid to insulin resistance as a distinct cause of cardiac dysfunction and heart failure in diabetic patients. A study of Swedish patients without prior cardiac dysfunction found that insulin resistance predicted the subsequent onset of heart failure independently of established risk factors (Ingelsson et al., 2005). In another clinical study, the plasma level of proinsulin (a marker of insulin resistance) was found to be higher in patients who subsequently developed heart failure than in control patients 20 years before the actual diagnosis of heart failure (Arnlöv et al., 2001). These findings indicate that insulin resistance precedes heart failure rather than being a consequence of it. Evidence has emerged that myocardial insulin resistance is central to altered metabolism in the failing heart and may play a crucial role in the development of heart failure (Ashrafian et al., 2007; Lopaschuk et al., 2007; Witteles and Fowler, 2008). The adaptive response of the failing heart involves a complex series of enzymatic shifts and changes in the regulation of transcriptional factors, which result in an increase of glucose metabolism and a decrease of fatty acid metabolism

to maximize the efficacy of energy production (Neubauer, 2007). Insulin resistance of the myocardium inhibits these adaptive responses, leading to increased reliance on fatty acid metabolism. This increases oxygen consumption and decreases cardiac function, raising the potential for lipotoxicity in the heart (Sharma et al., 2007; Young et al., 2002). Another line of evidence indicates that insulin signaling is upregulated in the failing heart and that excessive cardiac insulin signaling exacerbates systolic dysfunction (Shimizu et al., 2010).

Moreover, there is increasing evidence that heart failure reciprocally augments the risk of insulin resistance and clinical diabetes (Ashrafian et al., 2007). Insulin resistance and abnormal glucose metabolism are very common in heart failure patients, being identified in 43% of these patients, and such abnormalities are associated with decreased cardiac function (Suskin et al., 2000). Surprisingly, the link between heart failure and insulin resistance grows stronger when patients with ischemic heart disease are excluded (Witteles and Fowler, 2008). Heart failure also predicts the development of type 2 diabetes in a graded way (Tenenbaum et al., 2003). Although the above mentioned clinical evidence supports a role of insulin resistance in the occurrence of heart failure, evidence for the reciprocal statement that heart failure promotes insulin resistance is largely associative. Moreover, the role of heart failure in the promotion of insulin resistance has been demonstrated by only a few animal studies (Nikolaidis et al., 2004; Shimizu et al., 2010) and the underlying mechanisms are largely speculative.

Here, we studied the role of heart failure in the development of insulin resistance and sought to elucidate the molecular mechanisms involved. We found that insulin resistance developed in two murine models of heart failure, a chronic pressure overload model and a myocardial infarction model. Heart failure markedly upregulated p53 expression in adipose tissue in association with increased inflammation of adipose tissue. Heart failure accelerated lipolysis in adipose tissue, whereas inhibition of lipolysis by sympathetic denervation or treatment with a lipase inhibitor significantly downregulated adipose tissue p53 expression and inflammation, thereby improving insulin resistance. Likewise, disruption of p53 activation in adipose tissue not only ameliorated inflammation in this tissue and improved insulin resistance but also improved cardiac dysfunction associated with heart failure. We conclude that heart failure upregulates p53 in adipose tissue by promoting lipolysis via activation of the sympathetic nervous system, leading to an inflammatory response of adipose tissue and insulin resistance. Our results indicate that inhibition of p53-induced adipose inflammation is a potential target for treating metabolic abnormalities and systolic dysfunction in patients with heart failure.

RESULTS

Pressure Overload Induces Adipose Tissue Inflammation and Insulin Resistance

To examine the effect of cardiac pressure overload on glucose homeostasis, we produced transverse aortic constriction (TAC) in 11-week-old mice. In this mouse model, systolic cardiac function deteriorated significantly along with left ventricular (LV) dilatation 2–6 weeks after surgery (Figure S1A available online). The insulin tolerance test (ITT) and the glucose tolerance test (GTT) showed that insulin sensitivity and glucose tolerance were impaired at 4–6 weeks after TAC (Figure 1A) without any change of food intake (Figure S1B). In patients with metabolic disorders, the recruitment of inflammatory macrophages to adipose tissue has been shown to increase the production of proinflammatory cytokines, such as tumor necrosis factor (TNF)-α and chemokine (C–C motif) ligand 2 (CCL2), also known as monocyte chemoattractant protein-1 (MCP-1), leading to the development of systemic insulin resistance (Hotamisligil et al., 1993; Kamei et al., 2006; Weisberg et al., 2003). Therefore, we investigated whether pressure overload provokes adipose tissue inflammation. Examination of hematoxylin- and eosin-stained sections demonstrated the infiltration of mononuclear cells into visceral fat, with most of these cells being identified as macrophages by immunofluorescent staining for Mac3 (Figure 1B). Consistent with these results, expression of a marker for macrophages (Egf-like module containing, mucin-like, hormone receptor-like 1; EMR1) and production of proinflammatory cytokines were significantly upregulated in the adipose tissue of TAC mice along with a decrease of adiponectin (Figure 1C) compared with sham-operated mice. Treatment of TAC mice with a neutralizing antibody for Tnf-α significantly improved insulin resistance and glucose intolerance, suggesting a crucial role in the upregulation of proinflammatory cytokines in the development of metabolic abnormalities during heart failure (Figure S1C).

Pressure Overload Increases Lipolysis and Induces p53-Dependent Inflammation in Adipose Tissue during Heart Failure

Computed tomography (CT) showed a significant decrease of visceral fat after the creation of pressure overload (Figure 1D). It is well accepted that sympathetic activity increases with heart failure (Floras, 2009), and norepinephrine regulates lipolysis in adipose tissue. We found that the norepinephrine levels of plasma and adipose tissue increased significantly and plasma fatty acid levels were markedly elevated in TAC mice compared with sham-operated mice, suggesting acceleration of lipolysis via the sympathetic nervous system in response to pressure overload (Figure 1E). It has been reported that exposure to an excess of fatty acids leads to p53 activation in various cells (Zeng et al., 2008) and that p53 is crucially involved in the regulation of adipose tissue inflammation in obese animals (Minamino et al., 2009). Therefore, we hypothesized that chronic pressure overload promotes lipolysis and the resultant increase of fatty acids leads to p53-induced inflammation in adipose tissue.

Consistent with this concept, we found that p53 expression was upregulated in the adipose tissue of TAC mice at 2–4 weeks after surgery and the change was sustained until 6 weeks (Figures 2A and S2A). To further investigate the role of adipose tissue p53 in the response to pressure overload, we performed TAC in adipocyte-specific p53 knockout (adipo-p53 KO) mice. The pressure overload-induced increase of p53 expression was attenuated in adipo-p53 KO mice compared with littermate controls (Figure S2B). Production of proinflammatory cytokines as well as cyclin-dependent kinase inhibitor 1A (*Cdkn1a*) expression was also decreased in adipo-p53 KO mice, along with a decline in the infiltration of macrophages into visceral fat

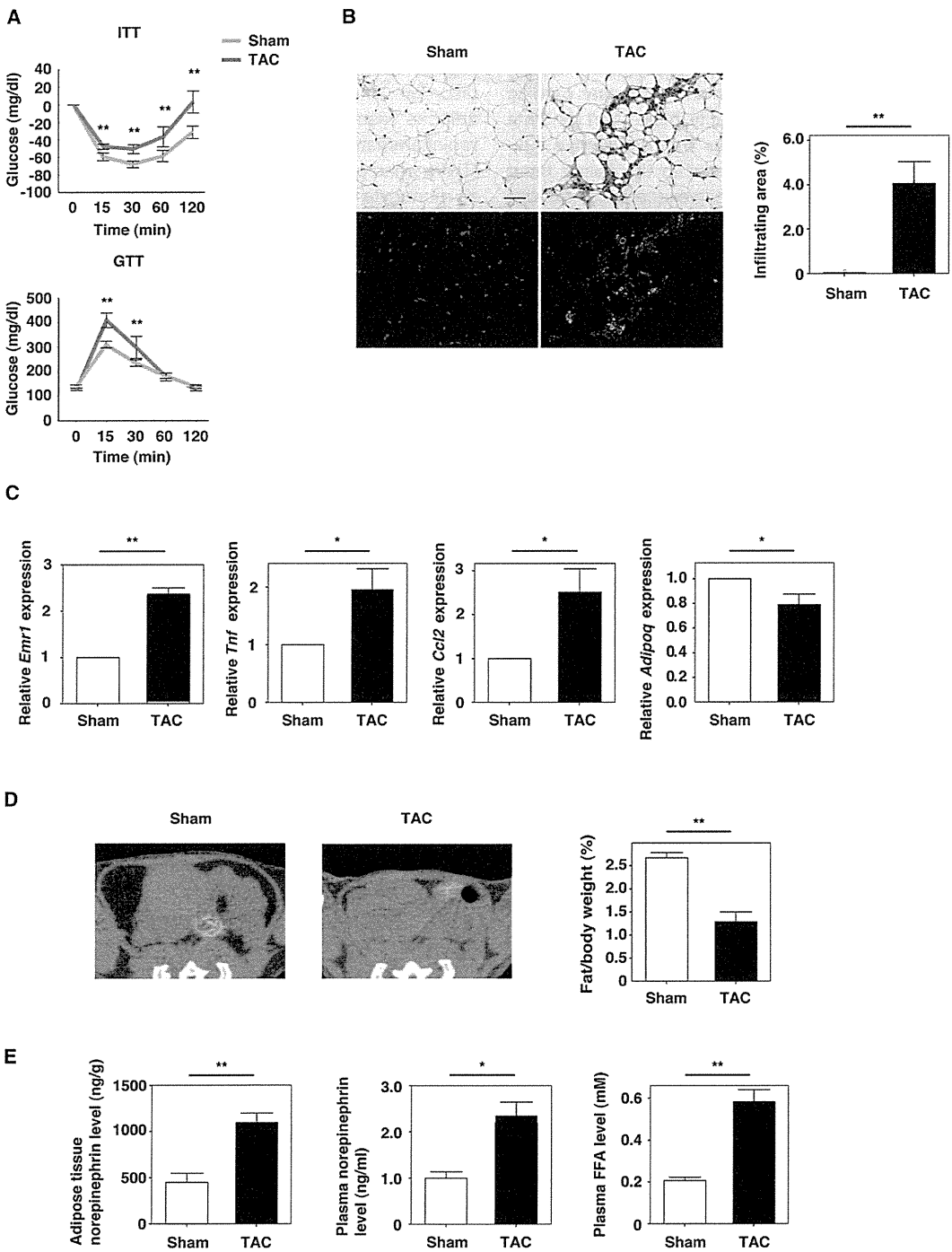

Figure 1. Pressure Overload Induces Systemic Insulin Resistance and Adipose Tissue Lipolysis and Inflammation

(A) Insulin tolerance test (ITT) and glucose tolerance test (GTT) in mice at 6 weeks after sham operation (Sham) or TAC (n = 30).

(B) Hematoxylin and eosin staining of adipose tissues of mice at 6 weeks after sham operation (Sham) or TAC (upper panel). In the lower panel, the infiltration of macrophages was evaluated by immunofluorescent staining for Mac3 (green). Nuclei were stained with Hoechst dye (blue). Scale bar, 50 μm. The right graph indicates the quantitative data on the infiltration of macrophages (n = 5).

(C) Real-time PCR assessing the expression of *Emr1*, *Tnf* (Tnfα), *Ccl2* (MCP1), and *Adipoq* (Adiponectin) levels in adipose tissues of mice at 6 weeks after sham operation (Sham) or TAC (n = 10).

(D) CT analysis of mice at 6 weeks after sham operation (Sham) or TAC. The graph shows the ratio of visceral fat tissue weight estimated by CT to whole body weight (n = 7).

(E) Norepinephrine level in adipose tissue (left) and plasma (middle), and plasma free fatty acid (FFA) level (right) of mice at 6 weeks after sham operation (Sham) or TAC (n = 10). Data are shown as the means ± S.E.M. *p < 0.05, **p < 0.01.

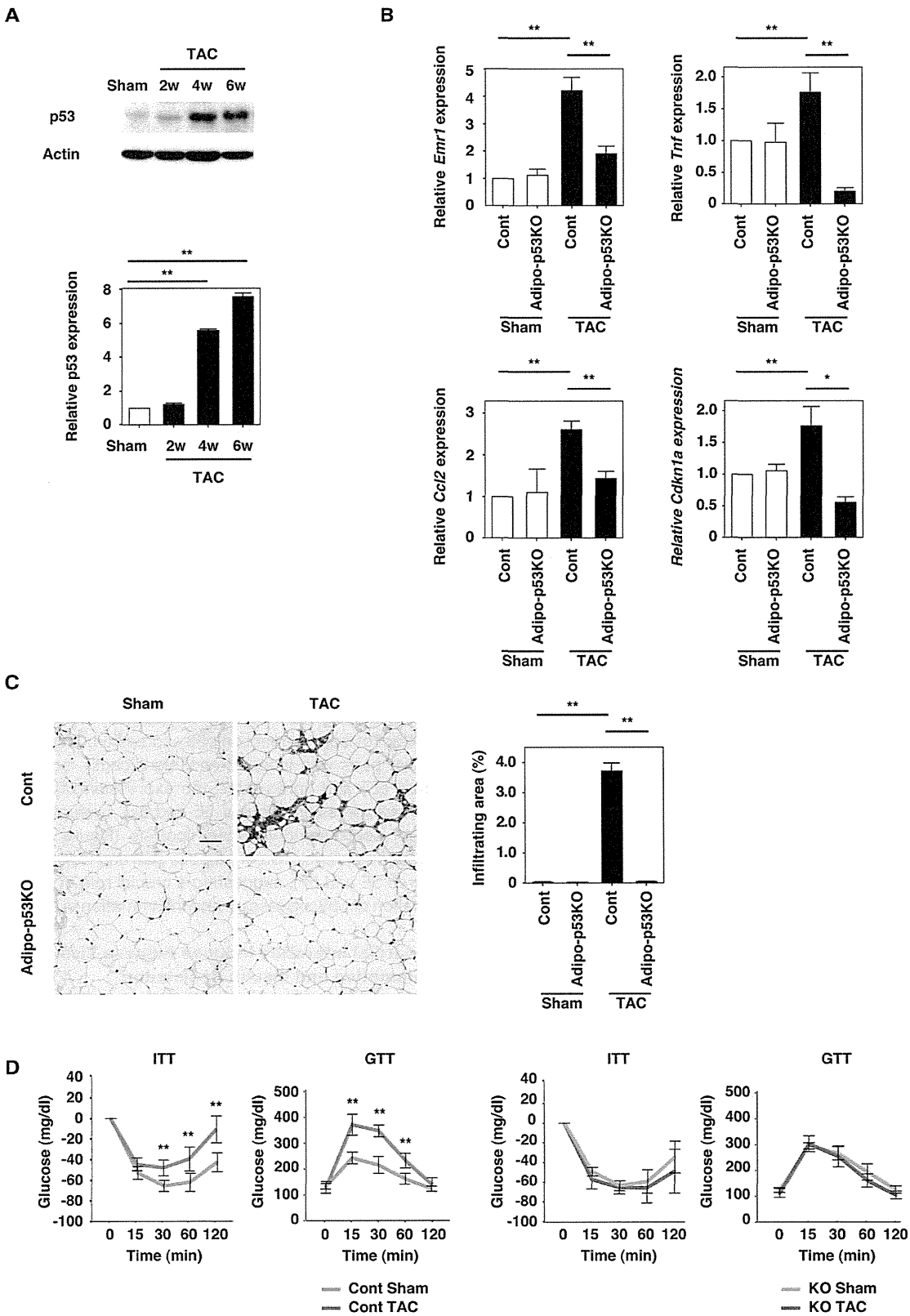
A
TAC
Sham 2w 4w 6w
p53
Actin
Relative p53 expression
Sham 2w 4w 6w
TAC
B
Relative Emr1 expression
Relative Tnf expression
Relative Ccl2 expression
Relative Cdkn1a expression
Cont
Adipo-p53KO
Sham
TAC
C
Sham
TAC
Cont
Adipo-p53KO
Infiltrating area (%)
D
ITT
GTT
Glucose (mg/dl)
Time (min)
Cont Sham
Cont TAC
KO Sham
KO TAC

(Figures 2B and 2C). Consequently, adipo-p53 KO mice showed improved insulin sensitivity and glucose tolerance after induction of pressure overload compared with littermate controls (Figure 2D) without any change of food intake (Figure S2C). These results suggest that p53 has a critical role in the regulation of adipose tissue inflammation and insulin resistance during pressure overload. In contrast, a decrease of fat mass and an increase of plasma free fatty acids were observed to a similar extent in both adipo-p53 KO and control mice after TAC (Figures S2D–S2F), suggesting that pressure overload accelerates lipolysis in a p53-independent manner.

Pressure Overload Promotes Lipolysis via the Sympathetic Nervous System

We inhibited sympathetic activity in epididymal fat tissue by surgical denervation and then performed TAC. As a result, surgical denervation effectively inhibited an increase of the norepinephrine level of adipose tissue and attenuated lipolysis after the onset of pressure overload (Figures S3A and S3B and data not shown). Histological examination of adipose tissue showed that infiltration of inflammatory cells after TAC was attenuated by denervation (Figures S3C and S3D). Likewise, disruption of the sympathetic efferent nerves significantly reduced pressure overload-induced upregulation of *Emr1*, a proinflammatory cytokine expression in adipose tissue (Figure 3A), and this reduction was associated with significant improvement of insulin resistance and glucose tolerance in TAC mice (Figure 3B). Surgical denervation attenuated pressure overload-induced upregulation of p53 and *Cdkn1a* expression in adipose tissue (Figures 3A and 3C). We also pharmacologically inhibited the sympathetic activity in adipose tissue by injecting guanethidine directly into epididymal fat and then performed TAC. As a result, pharmacological denervation also significantly inhibited lipolysis (Figures S3A and S3B) and attenuated upregulation of p53 and *Cdkn1a* expression and inflammation in adipose tissues (Figures S3C, S3D, S4A and S4B). Mice treated with guanethidine showed better insulin sensitivity and glucose tolerance after creation of pressure overload (Figure S4C), indicating that pressure overload-induced activation of the sympathetic nervous system accelerates lipolysis and, thus, leads to adipose tissue inflammation and insulin resistance in TAC mice.

Role of Lipolysis in the Regulation of Adipose p53 Expression and Inflammation

To examine the role of lipolysis in influencing adipose tissue expression of p53 and inflammation after TAC, we inhibited lipolysis by administering acipimox, a selective inhibitor of lipolysis, to mice with TAC. Treatment with acipimox markedly inhibited lipolysis and also reduced infiltration of inflammatory cells into adipose tissue during pressure overload (Figures S3A–S3D). Inhibition of lipolysis also significantly reduced pressure overload-induced upregulation of *Emr1* and proinflammatory cytokine production in adipose tissue (Figure 4A), along with significant improvement of insulin resistance and glucose intolerance in TAC mice (Figure 4B). Furthermore, treatment with acipimox attenuated pressure overload-induced upregulation of p53 and *Cdkn1a* expression in adipose tissue (Figures 4A and 4C), confirming a close relationship between lipolysis and p53 expression.

Next, we promoted lipolysis by administering isoproterenol to mice via an infusion pump. Treatment with isoproterenol significantly decreased the visceral fat mass and increased plasma fatty acid levels (Figures S5A–S5C) and increased p53 expression in adipose tissue (Figure 5A). Isoproterenol also induced adipose tissue inflammation (Figures 5B and 5C). To further investigate the role of lipolysis in the regulation of p53 expression and inflammation in adipose tissue, we tested the influence of deleting adipose triglyceride lipase (patatin-like phospholipase domain containing protein 2, encoded by *Pnpla2*; hereafter referred to as Atgl) on adipose tissue expression of p53. It has been reported that Atgl homozygous KO mice show massive accumulation of lipids in the heart, causing cardiac dysfunction and premature death (Haemmerle et al., 2006). When we generated TAC mice, we also noted that cardiac function was worse and LV enlargement was more marked in Atgl heterozygous KO mice compared with their littermates (Figure S5D). In fact, most of the KO mice died of heart failure within 4 weeks after TAC. Therefore, we utilized Atgl-deficient adipose tissue for ex vivo experiments. We cultured epididymal fat pad tissues from Atgl KO mice or wild-type littermates and examined the effect of isoproterenol on p53 expression. Treatment of wild-type fat pads with isoproterenol significantly induced lipolysis (Figure 5D) and upregulated the expression of both p53 and *Cdkn1a* expression (Figures 5E and 5F). Disruption of Atgl inhibited isoproterenol-induced lipolysis (Figure 5D) and prevented the upregulation of adipose p53 and *Cdkn1a* expression (Figures 5E and 5F), suggesting a crucial role of lipolysis in the regulation of p53 expression and inflammation in adipose tissue.

Myocardial Infarction Induces Adipose Tissue Inflammation and Insulin Resistance

To investigate whether myocardial infarction (MI) induced insulin resistance, we created MI in 11-week-old mice and assessed the animals 6 weeks after surgery. Insulin sensitivity and glucose tolerance were significantly impaired in MI mice compared with sham-operated mice (Figure S5E). Significant loss of fat tissue was also observed in MI mice (Figures S5F and S5G) and this was associated with upregulation of adipose

Figure 2. p53-Dependent Adipose Tissue Inflammation Provokes Systemic Insulin Resistance during Heart Failure

(A) Expression of p53 was examined in adipose tissues of mice by western blot analysis at indicated time points after sham operation (Sham) or TAC. Actin was used as an equal loading control. The graph indicates the quantitative data on p53 expression (n = 3).

(B) Real-time PCR assessing the expression of *Emr1*, *Tnf* (Tnfα), *Ccl2* (MCP1), and *Cdkn1a* (p21) levels in adipose tissue of adipocyte-specific p53-deficient mice (adipo-p53 KO) and littermate controls (Cont) at 6 weeks after sham operation or TAC procedure (n = 12).

(C) Hematoxylin and eosin staining of adipose tissues of adipocyte-specific p53-deficient mice (adipo-p53 KO) and littermate controls (Cont) at 6 weeks after sham operation (Sham) or TAC procedure. Scale bar, 50 μm. The right graph indicates the quantitative data on the infiltration of macrophages (n = 4).

(D) Insulin tolerance test (ITT) and glucose tolerance test (GTT) in adipocyte-specific p53-deficient mice (KO) and littermate controls (Cont) at 6 weeks after sham operation (Sham) or TAC procedure (n = 16). Data are shown as the means ± S.E.M. *$p < 0.05$, **$p < 0.01$.

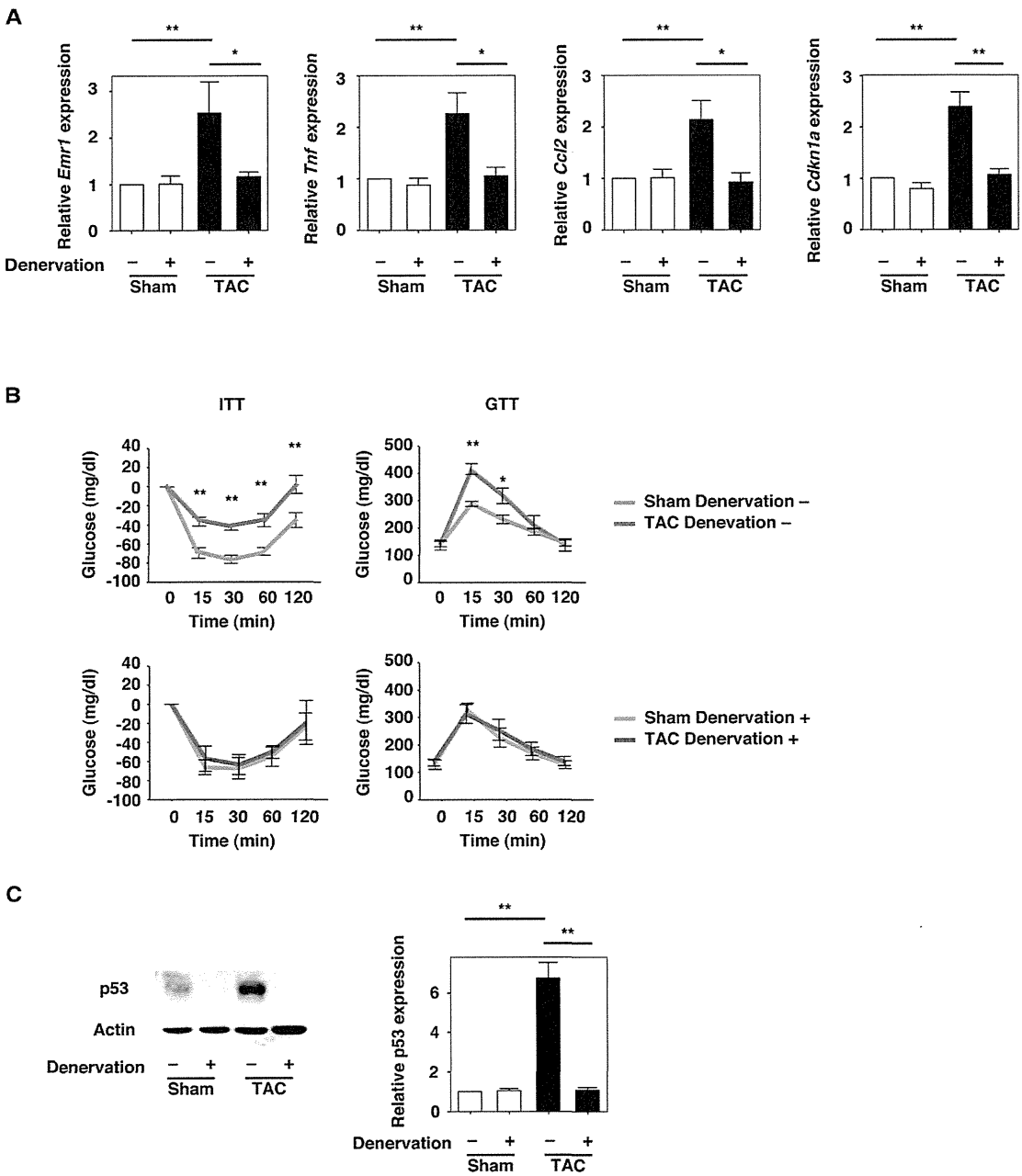

Figure 3. Surgical Transection of the Sympathetic Nerves Attenuates Adipose Tissue Inflammation and Systemic Insulin Resistance

(A) Real-time PCR assessing the expression of *Emr1*, *Tnf* (Tnfα), *Ccl2* (MCP1), and *Cdkn1a* (p21) levels in adipose tissues of mice at 6 weeks after sham operation (Sham) or TAC with or without surgical transection of the sympathetic nerves (Denervation) of epididymal fat (n = 8).

(B) Insulin tolerance test (ITT) and glucose tolerance test (GTT) of mice at 6 weeks after sham operation (Sham) or TAC with or without surgical denervation (n = 20).

(C) Western blot analysis of p53 in adipose tissues of mice at 6 weeks after sham operation (Sham) or TAC with or without surgical denervation. The right graph indicates the quantitative data on p53 expression (n = 3). Data are shown as the means ± S.E.M. *p < 0.05, **p < 0.01.

tissue p53 expression and inflammation (Figures S5H–S5J). Inhibition of p53 activation in adipose tissue by genetic disruption significantly attenuated inflammation of this tissue and improved metabolic abnormalities (Figures S5K and S5L). These results suggest that the same mechanism underlies insulin resistance associated with heart failure due to both pressure overload and MI.

Influence of Inhibiting p53-Induced Adipose Tissue Inflammation on Cardiac Function

To investigate whether inhibition of p53-induced adipose tissue inflammation could influence cardiac function in the development of heart failure, we performed TAC and monitored cardiac function in adipo-p53 KO mice. We found that adipo-p53 KO mice showed significantly better cardiac function and less LV

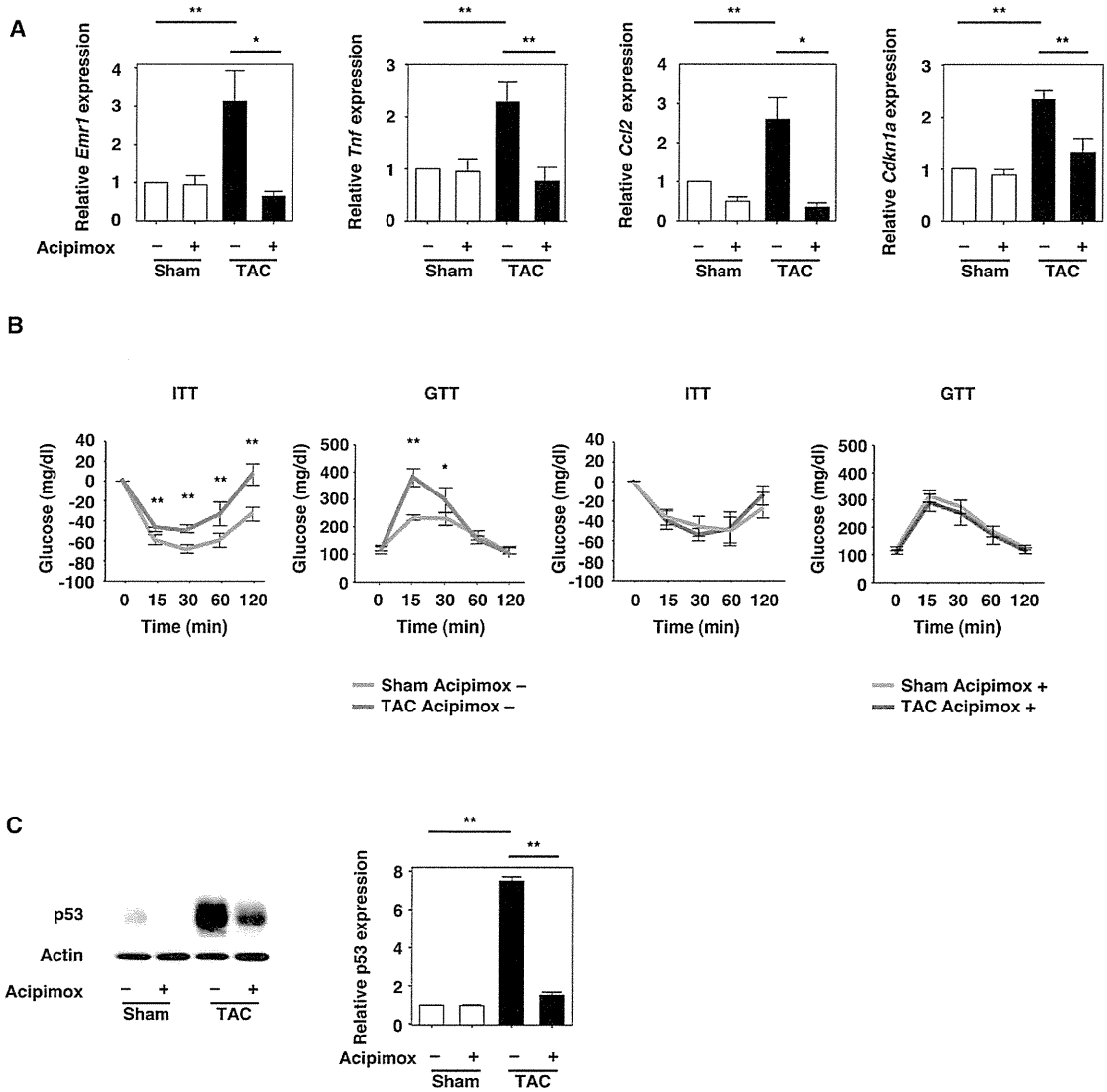

Figure 4. Treatment with a Lipolysis Inhibitor Ameliorates Adipose Tissue Inflammation and Systemic Insulin Resistance

(A) Real-time PCR assessing the expression of *Emr1*, *Tnf* (Tnfα), *Ccl2* (MCP1), and *Cdkn1a* (p21) levels in adipose tissue of mice at 6 weeks after sham operation (Sham) or TAC with or without acipimox treatment (n = 8).

(B) Insulin tolerance test (ITT) and glucose tolerance test (GTT) of mice at 6 weeks after sham operation (Sham) or TAC with or without acipimox treatment (n = 32).

(C) Western blot analysis of p53 in adipose tissues of mice at 6 weeks after sham operation (Sham) or TAC with or without acipimox treatment. Actin was used as an equal loading control. The right graph indicates the quantitative data on p53 expression (n = 3). Data are shown as the means ± S.E.M. *p < 0.05, **p < 0.01.

enlargement compared with their littermate controls (Figure 6A). They also showed better survival during the chronic phase of heart failure (Figure 6B). Similar results were observed in another model of heart failure induced by MI (Figure S6A). Furthermore, administration of a p53 inhibitor (pifithrin-α) into the adipose tissue of the TAC or MI model mice after the onset of heart failure improved cardiac dysfunction, as well as adipose tissue inflammation, and metabolic abnormalities (Figures 6C–6E and S6B–S6D), indicating that inhibition of p53 may be useful for the treatment of heart failure and its associated metabolic abnormalities. Moreover, we noted significant improvement of cardiac function after sympathetic nerve blockade (Figures S6E and S6F). However, treatment of TAC mice with acipimox was found to exacerbate cardiac dysfunction (Figure S6G), presumably because it impaired fatty acid metabolism and energy production in cardiomyocytes, as reported previously (Tuunanen et al., 2006).

Mechanism of p53-Induced Adipose Tissue Inflammation during Heart Failure

Because our results indicated that adrenergic activation induced lipolysis that upregulated p53 and promoted adipose tissue inflammation, we speculated that an excess of fatty acids might be involved in the upregulation of p53 in adipose tissue. Therefore, we examined the effect of palmitic acid on cultured preadipocytes. Treatment with palmitic acid significantly increased the

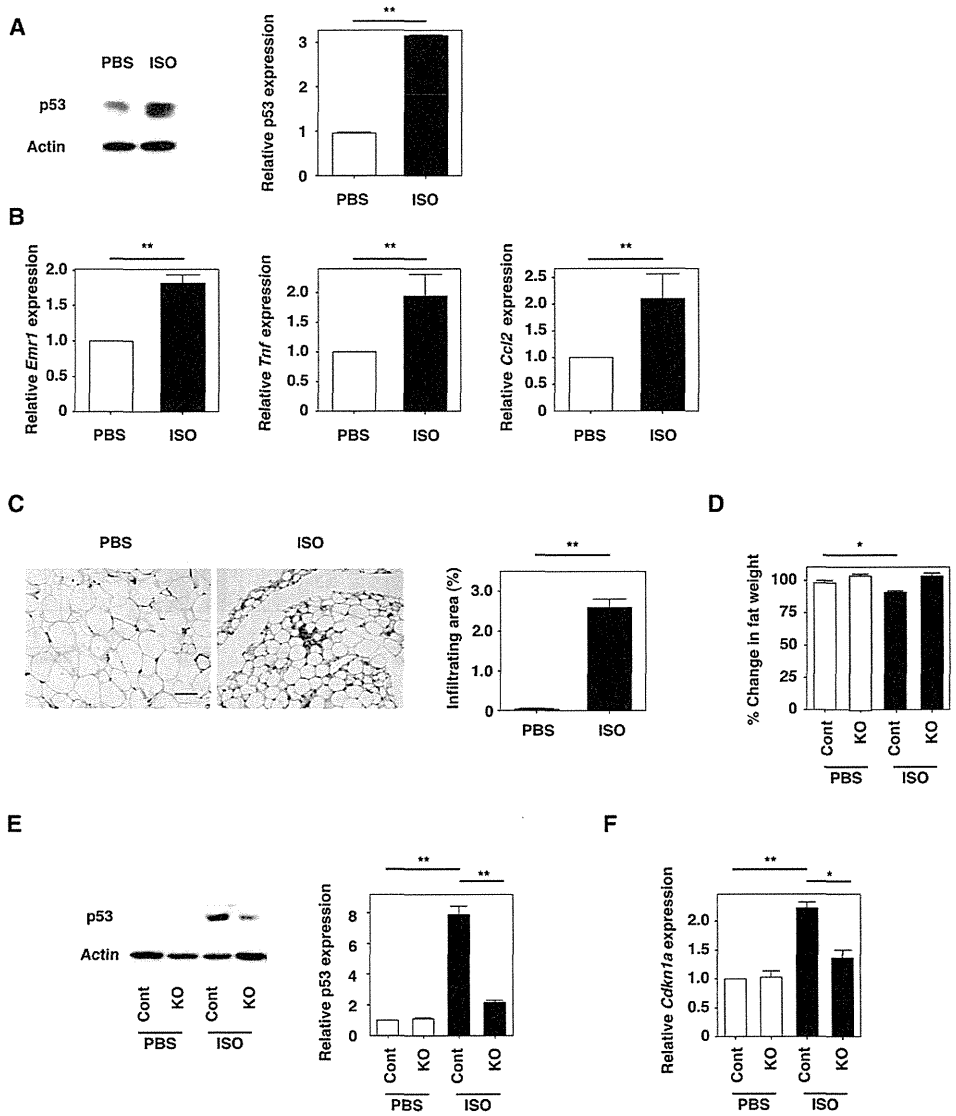

Figure 5. Role of Lipolysis in the Regulation of Adipose p53 Expression and Inflammation

(A) Western blot analysis of p53 in adipose tissues of wild-type mice treated with PBS or isoproterenol (ISO). Actin was used as an equal loading control. The right graph indicates the quantitative data on p53 expression (n = 3).

(B) Real-time PCR assessing the expression of *Emr1*, *Tnf* (Tnfα), and *Ccl2* (MCP1) levels in adipose tissues of wild-type mice treated with PBS or isoproterenol (ISO) (n = 8).

(C) Hematoxylin and eosin staining of adipose tissues of wild-type mice treated with PBS or isoproterenol (ISO). Scale bar, 50 μm. The right graph indicates the quantitative data on macrophage infiltration (n = 4).

(D) The changes in weight of adipose tissues isolated from Atgl-deficient mice (KO) and littermate controls (Cont) after treatment with PBS or isoproterenol (ISO) (n = 6).

(E) Expression of p53 was examined in adipose tissues of Atgl-deficient mice (KO) and littermate controls (Cont) treated with PBS or isoproterenol (ISO) by western blot analysis. The right graph indicates the quantitative data on p53 expression (n = 3).

(F) Real-time PCR assessing the expression of *Cdkn1a* (p21) level in adipose tissues isolated from Atgl-deficient mice (KO) and littermate controls (Cont) after treatment with PBS or isoproterenol (ISO) (n = 6). Data are shown as the means ± S.E.M. *$p < 0.05$, **$p < 0.01$.

intracellular level of reactive oxygen species (ROS) and caused DNA damage, as demonstrated by the increase of γH2AX, which in turn upregulated p53 expression (Figures 7A–7C, S7A, and S7B). This upregulation of p53 was associated with an increase of NF-κB activity and proinflammatory cytokine expression (Figures 7D and 7E). Because it has been reported that p53 enhances the activity of NF-κB, which regulates various cytokines including *TNF-α* and *CCL2* (Benoit et al., 2006; Ryan et al., 2000), we examined the relationship between p53 expression and NF-κB activation. We demonstrated that the disruption of p53 expression significantly attenuated palmitic acid-induced activation of NF-κB and upregulation of *Ccl2*

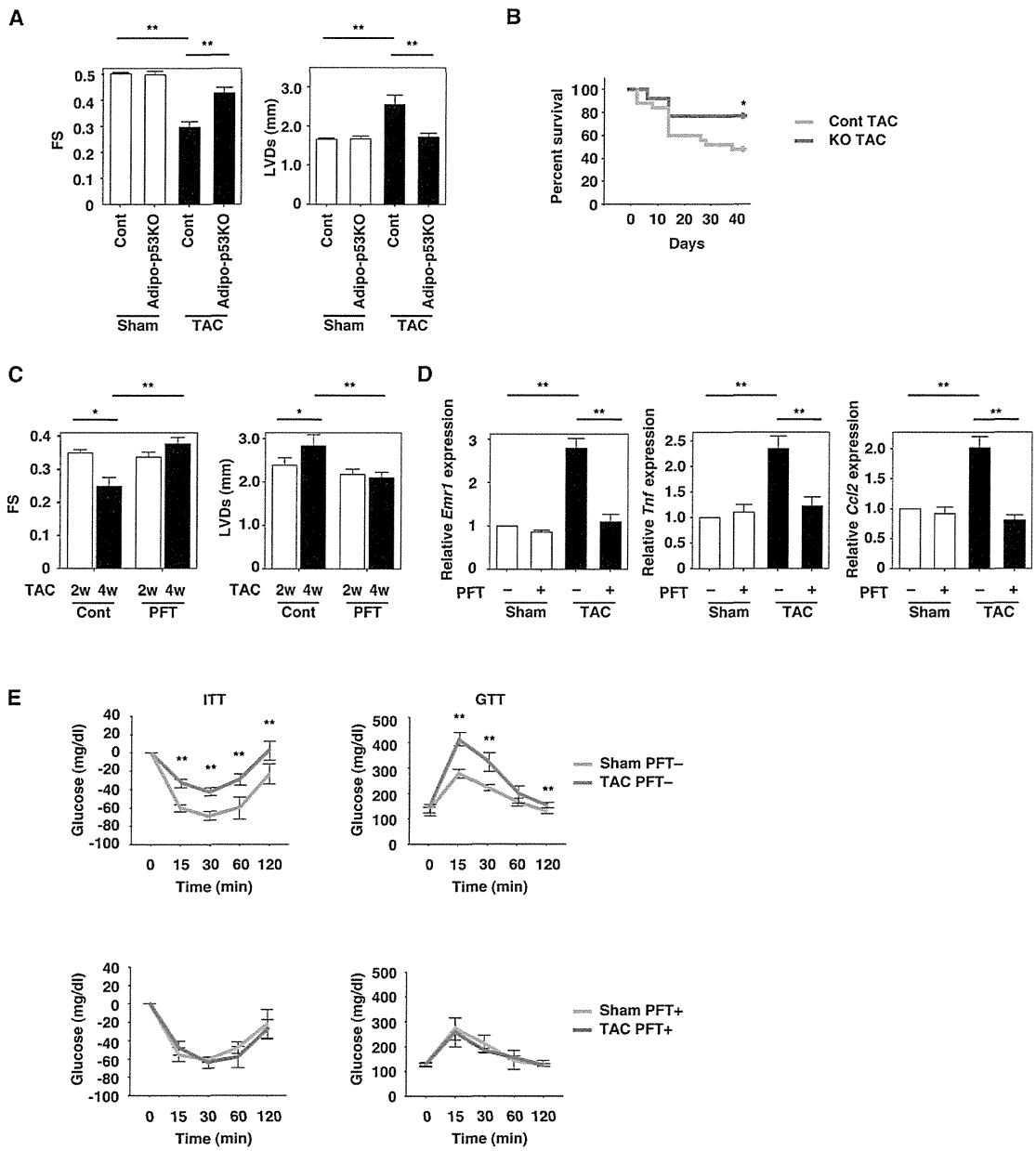

Figure 6. Influence of Inhibiting p53-Induced Adipose Tissue Inflammation on Cardiac Function

(A) Echocardiography to assess systolic function (FS) and ventricular size (LVDs) in adipocyte-specific p53-deficient mice (adipo-p53 KO) and littermate controls (Cont) at 6 weeks after sham operation or TAC (n = 8). FS, fractional shortening; LVDs, left ventricular end-systolic diameter.

(B) Survival rate of adipocyte-specific p53-deficient mice (adipo-p53 KO) and littermate controls (Cont) after TAC procedure (n = 25).

(C) Pifithrin-α (PFT) was administered into the adipose tissue of mice at 2–4 weeks after TAC, and systolic function (FS) and ventricular size (LVDs) were estimated before (2w, 2 weeks after TAC) and after (4w, 4 weeks after TAC) treatment by echocardiography (n = 5).

(D) Real-time PCR assessing the expression of *Emr1*, *Tnf* (Tnfα), and *Ccl2* (MCP1) levels in adipose tissue of mice at 4 weeks after sham operation or TAC with or without pifithrin-α (PFT) treatment (n = 4).

(E) Insulin tolerance test (ITT) and glucose tolerance test (GTT) of mice at 4 weeks after sham operation or TAC with or without pifithrin-α (PFT) treatment (n = 12). Data are shown as the means ± S.E.M. *p < 0.05, **p < 0.01.

(Figures 7D and 7E), whereas knockdown of the NF-κB component p50 markedly inhibited palmitic acid-induced upregulation of *Ccl2* (Figure 7E). In addition, treatment with an antioxidant inhibited palmitic acid-induced DNA damage and upregulation of p53 (Figures S7A and S7B). We also found that ROS and γH2AX expression were increased in the adipose tissue of mice with heart failure (Figures 7F and 7G). Furthermore, nuclear localization of p50 was enhanced in adipose tissue during heart failure (Figures 7H and S7C). This increase of nuclear p50 expression and the upregulation of proinflammatory cytokines

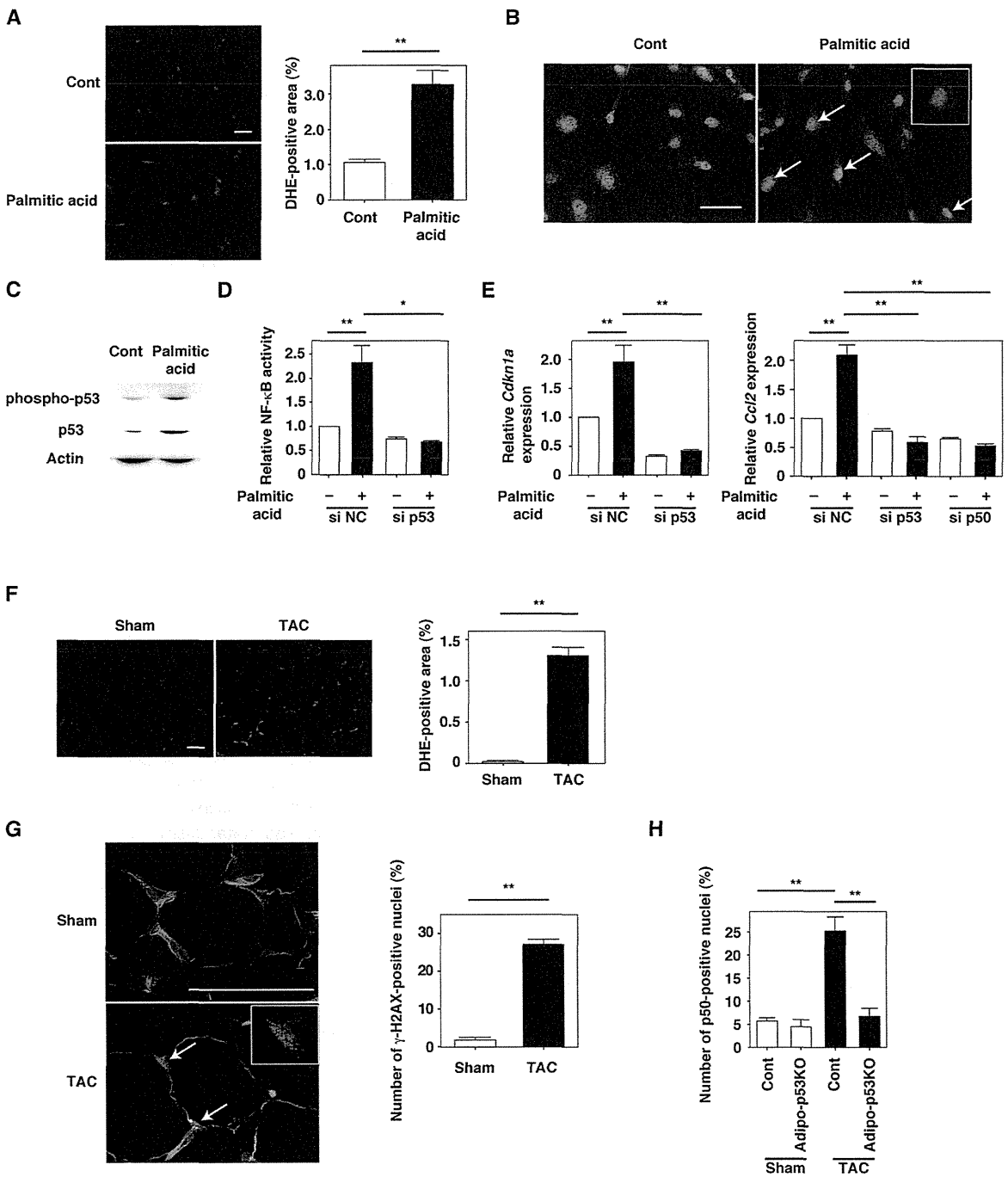

Figure 7. Mechanism of p53-Induced Adipose Tissue Inflammation during Heart Failure

(A) Dihydroethidium (DHE) staining (red) of preadipocytes treated with vehicle (Cont) or palmitic acid (500 μM) for 10 min. Nuclei were stained with Hoechst dye (blue). Scale bar indicates 50 μm. The right graph indicates the quantitative data on DHE-positive area (n = 4).

(B) Immunofluorescent staining for γ-H2AX (red) in preadipocytes treated with vehicle (Cont) or palmitic acid (500 μM) for 1 hr. Nuclei and plasma membranes were stained with Hoechst dye (blue) and Wheat Germ agglutinin lectin (green). Scale bar indicates 50 μm.

(C) Western blot analysis of phospho-p53 and p53 expression in preadipocytes treated with vehicle (Cont) or palmitic acid (500 μM).

(D) Small-interfering RNA targeting p53 (sip53) or negative control RNA (siNC) was introduced into preadipocytes treated with or without palmitic acid (500 μM) for 12 hr. The NF-κB activity was examined by luciferase assay (n = 5).

(E) Real-time PCR assessing the expression of *Cdkn1a* (p21) and *Ccl2* (MCP1) levels in preadipocytes prepared in Figure 7D (n = 9). The effect of small-interfering RNA targeting the NF-κB component p50 (sip50) on the expression of *Ccl2* (MCP1) was also examined (n = 9).

(F) Dihydroethidium (DHE) staining (red) in adipose tissue from sham-operated (Sham) and TAC mice. Nuclei were stained with Hoechst dye (blue). Scale bar indicates 20 μm. The right graph indicates the quantitative data on DHE-positive area (n = 5).

were inhibited by disruption of p53 in adipose tissue (Figures 2B, 7H, and S7C). Moreover, treatment with a lipolysis inhibitor significantly inhibited the heart failure-induced increase of ROS and nuclear p50 expression (Figures S7D and S7E). Inhibition of NF-κB activation in adipose tissue by BAY 11-7082 also significantly attenuated adipose tissue inflammation and improved metabolic abnormalities and cardiac dysfunction in TAC mice (Figures S7F–S7H). These results indicate that adrenergic activation by heart failure induces lipolysis in adipose tissue, which increases DNA damage due to ROS and thus upregulates p53. Activation of p53 then induces adipose tissue inflammation and metabolic abnormalities by upregulating the expression of NF-κB-dependent proinflammatory cytokines.

DISCUSSION

Although treatments that achieve neurohumoral antagonism have successfully reduced the morbidity and mortality of heart failure, the death rate remains unacceptably high (Kannel, 2000). Various metabolic abnormalities are associated with heart failure, and recent data have suggested that heart failure itself promotes adverse changes of metabolism, such as systemic insulin resistance (Ashrafian et al., 2007; Witteles and Fowler, 2008). Thus, a detrimental vicious cycle may be postulated, in which heart failure induces insulin resistance that in turn accelerates cardiac dysfunction (Opie, 2004). However, studies on the molecular mechanisms of such metabolic abnormalities in heart failure are largely preliminary and the results have sometimes been conflicting. In the present study, we demonstrated a causal role for heart failure in the development of insulin resistance by using two mouse models of heart failure, and we elucidated the underlying mechanisms. We found that the hyperadrenergic state of heart failure initiated a vicious metabolic cycle by promoting lipolysis in adipose tissue that increased the release of free fatty acids and upregulated p53 expression and proinflammatory cytokine production in adipose tissue, which then promoted systemic insulin resistance. Cardiac insulin resistance is considered to contribute to the development of heart failure. Because excessive cardiac insulin signaling has been reported to exacerbate systolic dysfunction in both TAC and MI models (Shimizu et al., 2010), hyperinsulinemia associated with systemic insulin resistance may also have a pathological role in heart failure until insulin resistance becomes evident in the myocardium. Inhibition of lipolysis by sympathetic denervation or by treatment with a lipolysis inhibitor improved insulin resistance in our heart failure model. Plasma free fatty acid levels were significantly elevated after the onset of heart failure, whereas this increase was attenuated by inhibition of lipolysis with acipimox, denervation, or guanethidine. Disruption of p53 in adipose tissue also markedly attenuated adipose inflammation and metabolic abnormalities associated with heart failure, whereas fatty acid levels were unaffected. Thus, adipose tissue inflammation rather than the increase of plasma free fatty acids per se is involved in the impairment of insulin sensitivity and glucose tolerance associated with heart failure. We also noted that p53 was modestly upregulated in the liver and skeletal muscle, presumably due to the increase of circulating free fatty acids. However, we did not detect a strong inflammatory response in those tissues under our experimental conditions (I. Shimizu and T. Minamino, unpublished data), suggesting that upregulation of adipose tissue p53 is more important for the development of metabolic abnormalities during heart failure. This concept is further supported by our finding that disruption of p53 activation in adipose tissue nearly normalized insulin resistance and glucose intolerance provoked by heart failure.

We observed that systolic cardiac function and survival with chronic heart failure were significantly better for adipo-p53 KO mice than their control littermates. Suppression of p53 activity in adipose tissue by administration of a p53 inhibitor after the onset of heart failure improved cardiac dysfunction and also reduced adipose tissue inflammation and metabolic abnormalities in both the TAC and MI models. Inhibition of NF-κB activity in adipose tissue also improved cardiac dysfunction, as well as adipose tissue inflammation and insulin resistance. Improvement of cardiac dysfunction by disruption of p53 in adipose tissue was not associated with a decrease of plasma free fatty acid levels. Systemic inhibition of lipolysis (Atgl deficiency or acipimox treatment) and disturbance of lipolysis in adipose tissue (denervation or guanethidine treatment) significantly reduced plasma free fatty acid levels (Haemmerle et al., 2006). However, the former intervention accelerated heart failure, whereas cardiac dysfunction was improved by the latter. Thus, the beneficial effect of inhibiting p53-induced adipose tissue inflammation on cardiac function is independent of changes in circulating free fatty acid levels, and lipolysis in cardiomyocytes appears to have a crucial role in cardiac metabolism and energy production. Although there is evidence suggesting that p53 has a protective role against damage due to ROS and lipotoxicity (Bazuine et al., 2009), our results indicate that chronic activation of p53 in adipose tissue causes inflammation and that inhibition of p53-induced adipose tissue inflammation is a potential target for treating metabolic abnormalities and systolic dysfunction in patients with heart failure.

Adipose tissue was traditionally considered to be a simple energy storage organ, but it is now appreciated that it also has endocrine functions and secretes a variety of factors referred to as adipokines (Donath and Shoelson, 2011; Hotamisligil, 2006; Ouchi et al., 2011). With high calorie intake, the size and number of adipocytes increase, and hypertrophic adipocytes shift the balance toward production of proinflammatory adipokines. This shift in the adipokine profile causes the modification of adipose tissue macrophages from the anti-inflammatory M2 type to the proinflammatory M1 type, and further increases the production of proinflammatory molecules, which in turn

(G) The number of γ-H2AX-positive nuclei (white arrows and inset) in adipose tissue of mice at 6 weeks after sham operation (Sham) or TAC procedure was estimated by immunofluorescent staining for γ-H2AX (red) (n = 5). Nuclei and plasma membranes were stained with Hoechst dye (blue) and Wheat Germ agglutinin lectin (green). Scale bar indicates 50 μm.

(H) The number of p50-positive nuclei in adipose tissue of adipocyte-specific p53-deficient mice (adipo-p53 KO) and littermate controls (Cont) at 6 weeks after sham operation (Sham) or TAC procedure was estimated by immunofluorescent staining for p50 (n = 6). Data are shown as the means ± S.E.M. *$p < 0.05$, **$p < 0.01$.

accelerates the recruitment of activated macrophages into inflamed fatty tissue. Adipokines produced by inflamed adipose tissue have been suggested to play a crucial role in the regulation of glucose and lipid metabolism and to contribute to the development of diabetes (Donath and Shoelson, 2011; Hotamisligil, 2006; Ouchi et al., 2011). It has been reported that excessive calorie intake leads to accumulation of ROS in adipose tissue and subsequently causes DNA damage that activates p53 (Minamino et al., 2009). In contrast to obesity, heart failure decreases body fat tissue mass by inducing lipolysis. Accelerated lipolysis and a subsequent increase of free fatty acids are likely to cause p53 activation because we found that the promotion of lipolysis by treatment with isoproterenol upregulated adipose tissue expression of p53, whereas inhibition of lipolysis by acipimox or disruption of lipase activity attenuated p53 expression. These results are consistent with a recent report describing that fasting-induced lipolysis promotes an immune response in murine adipose tissue (Kosteli et al., 2010). Various molecular mechanisms of p53 activation by heart failure may be postulated, including hypoxia, increased oxidative stress, and induction of endoplasmic reticulum stress (Harris and Levine, 2005; Schenk et al., 2008). Our in vitro and in vivo studies have indicated that an increase of free fatty acids causes ROS-induced DNA damage that upregulates p53 in adipose tissue. Activation of p53 then upregulates the expression of proinflammatory adipokines via the NF-κB signaling pathway and promotes systemic insulin resistance.

The β-blockers are competitive antagonists of β-adrenergic receptors. At one time, β-blockers were contraindicated in patients with heart failure due to their negative inotropic effect. However, several large-scale clinical trials demonstrated the efficacy of β-blockers for reducing morbidity and mortality in heart failure patients with impaired systolic function, so β-blockers are now recommended as first-line agent for these patients (Hjalmarson et al., 2000; Leizorovicz et al., 2002; Packer et al., 2001, 2002). A reduction of heart rate due to inhibition of cardiac β_1-adrenergic receptors is believed to be responsible for most of the therapeutic benefits associated with β-blocker treatment, although this is not the only mechanism of action that may be important in heart failure. It is interesting that treatment with a nonselective β-blocker (carvedilol) achieved a more marked improvement of survival in patients with chronic heart failure than treatment with a β_1-selective blocker (metoprolol) (Poole-Wilson et al., 2003), whereas new-onset diabetes was frequent in heart failure patients during treatment with the β_1-selective blocker (Torp-Pedersen et al., 2007). It has been reported that carvedilol antagonizes the β_3-adrenergic receptor as well as the $\beta_{1/2}$-adrenergic receptors (Schnabel et al., 2000). Taking our results together with these reports, it seems that inhibition of β_3-adrenergic activity in adipose tissue partially accounts for the better clinical outcome in patients treated with this nonselective β-blocker. Recent evidence has suggested that treatment with insulin sensitizers improves systolic function of the failing heart in animal models (Asakawa et al., 2002; Nemoto et al., 2005) but such treatment increases the incidence of heart failure in diabetic patients, presumably because of sodium retention (Home et al., 2009). Inhibition of p53-induced adipose tissue inflammation could be an alternative therapeutic target to block the metabolic vicious cycle in patients with heart failure.

EXPERIMENTAL PROCEDURES

Animal Models

All animal study protocols were approved by the Chiba University review board. C57BL/6 mice were purchased from the SLC Japan (Shizuoka, Japan). TAC and MI were performed in 11-week-old male mice as described previously (Harada et al., 2005; Sano et al., 2007). Sham-operated mice underwent the same procedure except for aortic constriction. Mice that expressed Cre recombinase in adipocytes (Fabp4-Cre) were purchased from Jackson Laboratories. We then crossed Fabp4-Cre mice (with a C57BL/6 background) with mice that carried floxed *Trp53* alleles with a C57BL/6 background (Marino et al., 2000) to generate adipocyte-specific p53 knockout mice. The genotype of littermate controls was Fabp4-Cre$^-$ *Trp53* $^{flox/flox}$. The generation and genotyping of Atgl-deficient mice has been described previously (Haemmerle et al., 2006). Surgical or chemical denervation was performed before TAC operation as described previously (Demas and Bartness, 2001; Foster and Bartness, 2006), with slight modification. In brief, the epididymal fat pad was gently separated from the skin and the abdominal wall by using a dissecting microscope. For surgical denervation, a drop of 1% toluidine blue was applied to the fat pad to facilitate visualization of the nerves. The nerves were then freed from the surrounding tissue and vasculature and cut in two or more locations, and the segments were removed to prevent possible reconnection. Chemical denervation was performed by the local injection of guanethidine sulfate (400 μg, Santa Cruz) into bilateral epididymal fat. Sham-operated mice for surgical denervation underwent the same procedure except for transection of the nerve. For the control group for chemical denervation, saline was injected into adipose tissue rather than guanethidine. Acipimox (Sigma) were provided in drinking water (at a concentration of 0.05%) for 6 weeks after TAC operation as described previously (Guo et al., 2009). Isoproterenol (30 mg/kg/day, Sigma) were delivered by infusion pump (DURECT Corporation) for 2 weeks as described previously (Iaccarino et al., 1999). The local injection of pifithrin-α (2.2 mg/kg/week, Carbiochem) or BAY 11-7082 (20 mg/kg/week, Carbiochem) into bilateral epididymal fat was performed to inhibit adipose p53 or NF-κB activity, respectively, from 2 weeks to 4 weeks after operation.

Physiological and Histological Analyses

Echocardiography was performed with a Vevo 770 High Resolution Imaging System (Visual Sonics Inc, Toronto, Ontario, Canada). To minimize variation of the data, the heart rate was always approximately 550–650 beats per minute when cardiac function was assessed. Epidydimal fat samples were harvested and fixed in 10% formalin overnight. The samples were embedded in paraffin and sectioned (Narabyouri research Co., Ltd). The sections were subjected to immunohistochemistry or HE staining. The antibodies used are Mac3-specific primary antibody (PharMingen) for macrophages, p50-specific primary antibody (Cell signaling), and phospho-H2AX-specific antibody (Cell signaling).

Laboratory Tests

For the intraperitoneal glucose tolerance test (IGTT), mice were starved for 6 hr and were given glucose intraperitoneally at a dose of 2 g / kg (body weight) in the early afternoon. For the insulin tolerance test, mice were given human insulin intraperitoneally (1 U / kg body weight) at 1:00 pm without starvation. Blood glucose levels were measured with a glucose analyzer (Roche Diagnostics). We analyzed free fatty acid (Biovision, Inc) and norepinephrine levels (LDN) by using ELISA-based immunoassay kits according to the manufacturer's instruction.

Western Blot Analysis

The lysates were resolved by SDS-polyacrylamide gel electrophoresis. Proteins were transferred to a polyvinylidene difluoride membrane (Millipore, Bedford, MA), which was incubated with the primary antibody followed by anti-rabbit or anti-mouse immunoglobulin-G conjugated with horseradish peroxidase (Jackson, West Grove, PA).

Cell Culture

Human preadipocytes were purchased from Sanko (Tokyo, Japan) and were cultured according to the manufacturer's instructions. NIH 3T3-L1 cells were cultured in high-glucose DMEM plus 10% fetal bovine serum.

Ex Vivo Culture

Epididymal fat was extracted from Atgl-deficient or littermate mice at 17 weeks of age. Freshly isolated fat pads (100–120 mg) were incubated in Dulbecco's modified Eagle's medium supplemented with 10% fetal bovine serum in the presence of isoproterenol (10 μM) for 48 hr. Fat pads were treated with PBS instead of isoproterenol in the control group.

Statistical Analysis

Data are shown as the mean ± SEM. Differences between groups were examined by Student's t-test or ANOVA followed by Bonferroni's correction for comparison of means. For survival analysis, the Kaplan-Meier method and log-rank test were used. For all analyses, $p < 0.05$ was considered statistically significant.

SUPPLEMENTAL INFORMATION

Supplemental Information includes Supplemental Experimental Procedures and seven figures and can be found with this article online at doi:10.1016/j.cmet.2011.12.006.

ACKNOWLEDGMENTS

We thank A. Berns (The Netherlands Cancer Institute) for floxed p53 mice, T. Fujita (The Tokyo Metropolitan Institute of Medical Science) for reagents, and E .Takahashi, M. Iijima, and I. Sakamoto for their excellent technical assistance. This work was supported by a Grant-in-Aid for Scientific Research from the Ministry of Education, Culture, Sports, Science and Technology of Japan and grants from the Ono Medical Research Foundation; the Uehara Memorial Foundation; the Daiichi-Sankyo Foundation of Life Science; the NOVARTIS Foundation for the Promotion Science; the Japan Diabetes Foundation; the Mitsui Life Social Welfare Foundation; the Naito Foundation; the Japanese Society of Anti-Aging Medicine; and the Mitsubishi Pharma Research Foundation (to T.M.); a Grant-in-Aid for Scientific Research from the Ministry of Education, Science, Sports, and Culture and Health and Labor Sciences Research Grants (to I.K.); and a Grant-in-Aid for Scientific Research from the Ministry of Education, Science, Sports, and Culture, and Health and a grant from the Uehara Memorial Foundation, Takeda Science Foundation, and Kowa Life Science Foundation (to I.S.).

Received: June 10, 2011
Revised: October 27, 2011
Accepted: December 9, 2011
Published online: January 3, 2012

REFERENCES

Arnlöv, J., Lind, L., Zethelius, B., Andrén, B., Hales, C.N., Vessby, B., and Lithell, H. (2001). Several factors associated with the insulin resistance syndrome are predictors of left ventricular systolic dysfunction in a male population after 20 years of follow-up. Am. Heart J. *142*, 720–724.

Asakawa, M., Takano, H., Nagai, T., Uozumi, H., Hasegawa, H., Kubota, N., Saito, T., Masuda, Y., Kadowaki, T., and Komuro, I. (2002). Peroxisome proliferator-activated receptor gamma plays a critical role in inhibition of cardiac hypertrophy in vitro and in vivo. Circulation *105*, 1240–1246.

Ashrafian, H., Frenneaux, M.P., and Opie, L.H. (2007). Metabolic mechanisms in heart failure. Circulation *116*, 434–448.

Bazuine, M., Stenkula, K.G., Cam, M., Arroyo, M., and Cushman, S.W. (2009). Guardian of corpulence: a hypothesis on p53 signaling in the fat cell. Clin. Lipidol. *4*, 231–243.

Benoit, V., de Moraes, E., Dar, N.A., Taranchon, E., Bours, V., Hautefeuille, A., Tanière, P., Chariot, A., Scoazec, J.Y., de Moura Gallo, C.V., et al. (2006). Transcriptional activation of cyclooxygenase-2 by tumor suppressor p53 requires nuclear factor-kappaB. Oncogene *25*, 5708–5718.

Demas, G.E., and Bartness, T.J. (2001). Novel method for localized, functional sympathetic nervous system denervation of peripheral tissue using guanethidine. J. Neurosci. Methods *112*, 21–28.

Donath, M.Y., and Shoelson, S.E. (2011). Type 2 diabetes as an inflammatory disease. Nat. Rev. Immunol. *11*, 98–107.

Edwards, M.G., Anderson, R.M., Yuan, M., Kendziorski, C.M., Weindruch, R., and Prolla, T.A. (2007). Gene expression profiling of aging reveals activation of a p53-mediated transcriptional program. BMC Genomics *8*, 80.

Floras, J.S. (2009). Sympathetic nervous system activation in human heart failure: clinical implications of an updated model. J. Am. Coll. Cardiol. *54*, 375–385.

Foster, M.T., and Bartness, T.J. (2006). Sympathetic but not sensory denervation stimulates white adipocyte proliferation. Am. J. Physiol. Regul. Integr. Comp. Physiol. *291*, R1630–R1637.

Guo, W., Wong, S., Pudney, J., Jasuja, R., Hua, N., Jiang, L., Miller, A., Hruz, P.W., Hamilton, J.A., and Bhasin, S. (2009). Acipimox, an inhibitor of lipolysis, attenuates atherogenesis in LDLR-null mice treated with HIV protease inhibitor ritonavir. Arterioscler. Thromb. Vasc. Biol. *29*, 2028–2032.

Haemmerle, G., Lass, A., Zimmermann, R., Gorkiewicz, G., Meyer, C., Rozman, J., Heldmaier, G., Maier, R., Theussl, C., Eder, S., et al. (2006). Defective lipolysis and altered energy metabolism in mice lacking adipose triglyceride lipase. Science *312*, 734–737.

Harada, M., Qin, Y., Takano, H., Minamino, T., Zou, Y., Toko, H., Ohtsuka, M., Matsuura, K., Sano, M., Nishi, J., et al. (2005). G-CSF prevents cardiac remodeling after myocardial infarction by activating the Jak-Stat pathway in cardiomyocytes. Nat. Med. *11*, 305–311.

Harris, S.L., and Levine, A.J. (2005). The p53 pathway: positive and negative feedback loops. Oncogene *24*, 2899–2908.

Hjalmarson, A., Goldstein, S., Fagerberg, B., Wedel, H., Waagstein, F., Kjekshus, J., Wikstrand, J., El Allaf, D., Vítovec, J., Aldershvile, J., et al; MERIT-HF Study Group. (2000). Effects of controlled-release metoprolol on total mortality, hospitalizations, and well-being in patients with heart failure: the Metoprolol CR/XL Randomized Intervention Trial in congestive heart failure (MERIT-HF). JAMA *283*, 1295–1302.

Home, P.D., Pocock, S.J., Beck-Nielsen, H., Curtis, P.S., Gomis, R., Hanefeld, M., Jones, N.P., Komajda, M., and McMurray, J.J.; RECORD Study Team. (2009). Rosiglitazone evaluated for cardiovascular outcomes in oral agent combination therapy for type 2 diabetes (RECORD): a multicentre, randomised, open-label trial. Lancet *373*, 2125–2135.

Hotamisligil, G.S. (2006). Inflammation and metabolic disorders. Nature *444*, 860–867.

Hotamisligil, G.S., Shargill, N.S., and Spiegelman, B.M. (1993). Adipose expression of tumor necrosis factor-alpha: direct role in obesity-linked insulin resistance. Science *259*, 87–91.

Iaccarino, G., Dolber, P.C., Lefkowitz, R.J., and Koch, W.J. (1999). Bbeta-adrenergic receptor kinase-1 levels in catecholamine-induced myocardial hypertrophy: regulation by beta- but not alpha1-adrenergic stimulation. Hypertension *33*, 396–401.

Ingelsson, E., Sundström, J., Arnlöv, J., Zethelius, B., and Lind, L. (2005). Insulin resistance and risk of congestive heart failure. JAMA *294*, 334–341.

Kamei, N., Tobe, K., Suzuki, R., Ohsugi, M., Watanabe, T., Kubota, N., Ohtsuka-Kowatari, N., Kumagai, K., Sakamoto, K., Kobayashi, M., et al. (2006). Overexpression of monocyte chemoattractant protein-1 in adipose tissues causes macrophage recruitment and insulin resistance. J. Biol. Chem. *281*, 26602–26614.

Kannel, W.B. (2000). Incidence and epidemiology of heart failure. Heart Fail. Rev. *5*, 167–173.

Kosteli, A., Sugaru, E., Haemmerle, G., Martin, J.F., Lei, J., Zechner, R., and Ferrante, A.W., Jr. (2010). Weight loss and lipolysis promote a dynamic immune response in murine adipose tissue. J. Clin. Invest. *120*, 3466–3479.

Leizorovicz, A., Lechat, P., Cucherat, M., and Bugnard, F. (2002). Bisoprolol for the treatment of chronic heart failure: a meta-analysis on individual data of two placebo-controlled studies—CIBIS and CIBIS II. Cardiac Insufficiency Bisoprolol Study. Am. Heart J. *143*, 301–307.

Lopaschuk, G.D., Folmes, C.D., and Stanley, W.C. (2007). Cardiac energy metabolism in obesity. Circ. Res. *101*, 335–347.

Maier, B., Gluba, W., Bernier, B., Turner, T., Mohammad, K., Guise, T., Sutherland, A., Thorner, M., and Scrable, H. (2004). Modulation of mammalian life span by the short isoform of p53. Genes Dev. *18*, 306–319.

Marino, S., Vooijs, M., van Der Gulden, H., Jonkers, J., and Berns, A. (2000). Induction of medulloblastomas in p53-null mutant mice by somatic inactivation of Rb in the external granular layer cells of the cerebellum. Genes Dev. *14*, 994–1004.

Meek, D.W. (2009). Tumour suppression by p53: a role for the DNA damage response? Nat. Rev. Cancer *9*, 714–723.

Minamino, T., and Komuro, I. (2007). Vascular cell senescence: contribution to atherosclerosis. Circ. Res. *100*, 15–26.

Minamino, T., and Komuro, I. (2008). Vascular aging: insights from studies on cellular senescence, stem cell aging, and progeroid syndromes. Nat. Clin. Pract. Cardiovasc. Med. *5*, 637–648.

Minamino, T., Orimo, M., Shimizu, I., Kunieda, T., Yokoyama, M., Ito, T., Nojima, A., Nabetani, A., Oike, Y., Matsubara, H., et al. (2009). A crucial role for adipose tissue p53 in the regulation of insulin resistance. Nat. Med. *15*, 1082–1087.

Nemoto, S., Razeghi, P., Ishiyama, M., De Freitas, G., Taegtmeyer, H., and Carabello, B.A. (2005). PPAR-gamma agonist rosiglitazone ameliorates ventricular dysfunction in experimental chronic mitral regurgitation. Am. J. Physiol. Heart Circ. Physiol. *288*, H77–H82.

Neubauer, S. (2007). The failing heart—an engine out of fuel. N. Engl. J. Med. *356*, 1140–1151.

Nikolaidis, L.A., Sturzu, A., Stolarski, C., Elahi, D., Shen, Y.T., and Shannon, R.P. (2004). The development of myocardial insulin resistance in conscious dogs with advanced dilated cardiomyopathy. Cardiovasc. Res. *61*, 297–306.

Opie, L.H. (2004). The metabolic vicious cycle in heart failure. Lancet *364*, 1733–1734.

Ouchi, N., Parker, J.L., Lugus, J.J., and Walsh, K. (2011). Adipokines in inflammation and metabolic disease. Nat. Rev. Immunol. *11*, 85–97.

Packer, M., Coats, A.J., Fowler, M.B., Katus, H.A., Krum, H., Mohacsi, P., Rouleau, J.L., Tendera, M., Castaigne, A., Roecker, E.B., et al; Carvedilol Prospective Randomized Cumulative Survival Study Group. (2001). Effect of carvedilol on survival in severe chronic heart failure. N. Engl. J. Med. *344*, 1651–1658.

Packer, M., Fowler, M.B., Roecker, E.B., Coats, A.J., Katus, H.A., Krum, H., Mohacsi, P., Rouleau, J.L., Tendera, M., Staiger, C., et al; Carvedilol Prospective Randomized Cumulative Survival (COPERNICUS) Study Group. (2002). Effect of carvedilol on the morbidity of patients with severe chronic heart failure: results of the carvedilol prospective randomized cumulative survival (COPERNICUS) study. Circulation *106*, 2194–2199.

Poole-Wilson, P.A., Swedberg, K., Cleland, J.G., Di Lenarda, A., Hanrath, P., Komajda, M., Lubsen, J., Lutiger, B., Metra, M., Remme, W.J., et al; Carvedilol Or Metoprolol European Trial Investigators. (2003). Comparison of carvedilol and metoprolol on clinical outcomes in patients with chronic heart failure in the Carvedilol Or Metoprolol European Trial (COMET): randomised controlled trial. Lancet *362*, 7–13.

Royds, J.A., and Iacopetta, B. (2006). p53 and disease: when the guardian angel fails. Cell Death Differ. *13*, 1017–1026.

Ryan, K.M., Ernst, M.K., Rice, N.R., and Vousden, K.H. (2000). Role of NF-kappaB in p53-mediated programmed cell death. Nature *404*, 892–897.

Sano, M., Minamino, T., Toko, H., Miyauchi, H., Orimo, M., Qin, Y., Akazawa, H., Tateno, K., Kayama, Y., Harada, M., et al. (2007). p53-induced inhibition of Hif-1 causes cardiac dysfunction during pressure overload. Nature *446*, 444–448.

Schenk, S., Saberi, M., and Olefsky, J.M. (2008). Insulin sensitivity: modulation by nutrients and inflammation. J. Clin. Invest. *118*, 2992–3002.

Schnabel, P., Maack, C., Mies, F., Tyroller, S., Scheer, A., and Böhm, M. (2000). Binding properties of beta-blockers at recombinant beta1-, beta2-, and beta3-adrenoceptors. J. Cardiovasc. Pharmacol. *36*, 466–471.

Sharma, N., Okere, I.C., Duda, M.K., Chess, D.J., O'Shea, K.M., and Stanley, W.C. (2007). Potential impact of carbohydrate and fat intake on pathological left ventricular hypertrophy. Cardiovasc. Res. *73*, 257–268.

Shimizu, I., Minamino, T., Toko, H., Okada, S., Ikeda, H., Yasuda, N., Tateno, K., Moriya, J., Yokoyama, M., Nojima, A., et al. (2010). Excessive cardiac insulin signaling exacerbates systolic dysfunction induced by pressure overload in rodents. J. Clin. Invest. *120*, 1506–1514.

Suskin, N., McKelvie, R.S., Burns, R.J., Latini, R., Pericak, D., Probstfield, J., Rouleau, J.L., Sigouin, C., Solymoss, C.B., Tsuyuki, R., et al. (2000). Glucose and insulin abnormalities relate to functional capacity in patients with congestive heart failure. Eur. Heart J. *21*, 1368–1375.

Tenenbaum, A., Motro, M., Fisman, E.Z., Leor, J., Freimark, D., Boyko, V., Mandelzweig, L., Adler, Y., Sherer, Y., and Behar, S. (2003). Functional class in patients with heart failure is associated with the development of diabetes. Am. J. Med. *114*, 271–275.

Torp-Pedersen, C., Metra, M., Charlesworth, A., Spark, P., Lukas, M.A., Poole-Wilson, P.A., Swedberg, K., Cleland, J.G., Di Lenarda, A., Remme, W.J., and Scherhag, A.; COMET investigators. (2007). Effects of metoprolol and carvedilol on pre-existing and new onset diabetes in patients with chronic heart failure: data from the Carvedilol Or Metoprolol European Trial (COMET). Heart *93*, 968–973.

Tuunanen, H., Engblom, E., Naum, A., Någren, K., Hesse, B., Airaksinen, K.E., Nuutila, P., Iozzo, P., Ukkonen, H., Opie, L.H., and Knuuti, J. (2006). Free fatty acid depletion acutely decreases cardiac work and efficiency in cardiomyopathic heart failure. Circulation *114*, 2130–2137.

Tyner, S.D., Venkatachalam, S., Choi, J., Jones, S., Ghebranious, N., Igelmann, H., Lu, X., Soron, G., Cooper, B., Brayton, C., et al. (2002). p53 mutant mice that display early ageing-associated phenotypes. Nature *415*, 45–53.

Vousden, K.H., and Lane, D.P. (2007). p53 in health and disease. Nat. Rev. Mol. Cell Biol. *8*, 275–283.

Vousden, K.H., and Prives, C. (2009). Blinded by the Light: The Growing Complexity of p53. Cell *137*, 413–431.

Vousden, K.H., and Ryan, K.M. (2009). p53 and metabolism. Nat. Rev. Cancer *9*, 691–700.

Weisberg, S.P., McCann, D., Desai, M., Rosenbaum, M., Leibel, R.L., and Ferrante, A.W., Jr. (2003). Obesity is associated with macrophage accumulation in adipose tissue. J. Clin. Invest. *112*, 1796–1808.

Witteles, R.M., and Fowler, M.B. (2008). Insulin-resistant cardiomyopathy clinical evidence, mechanisms, and treatment options. J. Am. Coll. Cardiol. *51*, 93–102.

Young, M.E., McNulty, P., and Taegtmeyer, H. (2002). Adaptation and maladaptation of the heart in diabetes: Part II: potential mechanisms. Circulation *105*, 1861–1870.

Zeng, L., Wu, G.Z., Goh, K.J., Lee, Y.M., Ng, C.C., You, A.B., Wang, J., Jia, D., Hao, A., Yu, Q., and Li, B. (2008). Saturated fatty acids modulate cell response to DNA damage: implication for their role in tumorigenesis. PLoS ONE *3*, e2329.

Circulation
JOURNAL OF THE AMERICAN HEART ASSOCIATION

American Heart Association®
Learn and Live℠

Does Stringent Restrictive Annuloplasty for Functional Mitral Regurgitation Cause Functional Mitral Stenosis and Pulmonary Hypertension?

Satoshi Kainuma, Kazuhiro Taniguchi, Takashi Daimon, Taichi Sakaguchi, Toshihiro Funatsu, Haruhiko Kondoh, Shigeru Miyagawa, Koji Takeda, Yasuhiro Shudo, Takafumi Masai, Shinichi Fujita, Masami Nishino, Yoshiki Sawa and Osaka Cardiovascular Surgery Research (OSCAR) Group

Circulation 2011, 124:S97-S106
doi: 10.1161/CIRCULATIONAHA.110.013037
Circulation is published by the American Heart Association. 7272 Greenville Avenue, Dallas, TX 72514
 Print ISSN: 0009-7322. Online ISSN: 1524-4539

Does Stringent Restrictive Annuloplasty for Functional Mitral Regurgitation Cause Functional Mitral Stenosis and Pulmonary Hypertension?

Satoshi Kainuma, MD; Kazuhiro Taniguchi, MD, PhD; Takashi Daimon, PhD; Taichi Sakaguchi, MD, PhD; Toshihiro Funatsu, MD, PhD; Haruhiko Kondoh, MD, PhD; Shigeru Miyagawa, MD, PhD; Koji Takeda, MD, PhD; Yasuhiro Shudo, MD; Takafumi Masai, MD, PhD; Shinichi Fujita, CE; Masami Nishino, MD, PhD; Yoshiki Sawa, MD, PhD; Osaka Cardiovascular Surgery Research (OSCAR) Group

Background—It remains controversial whether restrictive mitral annuloplasty (RMA) for functional mitral regurgitation (MR) can induce functional mitral stenosis (MS) that may cause postoperative residual pulmonary hypertension (PH).

Methods and Results—One hundred eight patients with left ventricular (LV) dysfunction and severe MR underwent RMA with stringent downsizing of the mitral annulus. Systolic pulmonary artery pressure (PAP) and mitral valve performance variables were determined by Doppler echocardiography prospectively and 1 month after RMA. Fifty-eight patients underwent postoperative hemodynamic measurements. Postoperative echocardiography showed a mean pressure half-time of 92±14 ms, a transmitral mean gradient of 2.9±1.1 mm Hg, and a mitral valve effective orifice area of 2.4±0.4 cm^2, consistent with functional MS. Doppler-derived systolic PAP was 32±8 mm Hg, which correlated weakly with the transmitral mean gradient (ρ=0.23, P=0.02). Postoperative cardiac catheterization also showed significant improvements in LV volume and systolic function, pulmonary capillary wedge pressure, cardiac index, and systolic PAP; the latter was associated with LV end-diastolic pressure [standardized partial regression coefficient (SPRC)=0.51], pulmonary vascular resistance (SPRC=0.47), cardiac index (SPRC=0.37), and transmitral pressure gradient (SPRC=0.20). In a multivariate Cox proportional hazard model, postoperative PH (systolic PAP >40 mm Hg), but not mitral valve performance variables, was strongly associated with adverse cardiac events.

Conclusions—RMA for functional MR resulted in varying degrees of functional MS. However, our data were more consistent with the residual PH being caused by LV dysfunction and pulmonary vascular disease than by the functional MS. The residual PH, not functional MS, was the major predictor of post-RMA adverse cardiac events. **(*Circulation*. 2011;124[suppl 1]:S97–S106.)**

Key Words: functional mitral regurgitation ■ cardiomyopathy ■ restrictive mitral annuloplasty ■ functional mitral stenosis ■ pulmonary hypertension ■ patient-prosthesis mismatch

Restrictive mitral annuloplasty (RMA), which involves the insertion of an undersized prosthetic ring, has become the preferred surgical option for the treatment of patients with medically uncontrollable, severe functional mitral regurgitation (MR). Previous studies[1–4] have shown that stringent RMA can effectively eliminate functional MR, resulting in reverse left ventricular (LV) remodeling, and improved symptoms, and survival in the great majority of patients.

In contrast to these beneficial effects of the RMA procedure, Magne et al[5] first reported that the insertion of such an undersized ring may induce an iatrogenic "functional" mitral stenosis (MS) similar to prosthesis-patient mismatch (PPM), a condition that is frequently found after mitral valve replacement with a small prosthetic valve.[6–8] The effective orifice area (EOA) of a prosthetic valve or annuloplasty ring is often too small in relation to body size, causing a mismatch between the EOA and the transmitral flow, and yielding relatively high gradients. Several recent studies have reported a high incidence of functional MS, in which the mitral valve area is less than 1.5 cm^2[9] or the mean pressure gradient is greater than 5 mm Hg, after RMA.[10] In contrast, most prior

From the Department of Cardiovascular Surgery (S.K., Ka.T., T.F., H.K.), Division of Cardiology (M.N.), and Clinical Echocardiography Section (S.F.), Japan Labor Health and Welfare Organization Osaka Rosai Hospital, Sakai, Osaka, Japan; the Department of Cardiovascular Surgery (S.K., T.S., S.M., Ko.T., Ya.S., Yo.S.), Osaka University Graduate School of Medicine, Suita, Osaka, Japan; the Department of Cardiovascular Surgery (T.M.), Sakurabashi Watanabe Hospital, Osaka, Japan; and the Department of Biostatistics (T.D.), Hyogo College of Medicine, Nishinomiya, Hyogo, Japan.

Presented at the 2010 American Heart Association meeting in Chicago, IL, November 12–16, 2010.

Correspondence to Yoshiki Sawa, MD, Department of Cardiovascular Surgery, Osaka University Graduate School of Medicine, Suita, Osaka 565-0871, Japan. E-mail Sawa@surg1.med.osaka-u.ac.jp

Circulation **is available at http://circ.ahajournals.org** **DOI: 10.1161/CIRCULATIONAHA.110.013037**